Monthly Notices of the ROYAL ASTRONOMICAL SOCIETY

MNRAS **533,** 3442–3456 (2024) https://doi.org/10.1093/mnras/stae1849
Advance Access publication 2024 July 31

ExoMol line lists – LX. Molecular line list for the ammonia isotopologue $^{15}NH_3$

Sergei N. Yurchenko ,★ Charles A. Bowesman, Ryan P. Brady , Elizabeth R. Guest, Kyriaki Kefala, Georgi B. Mitev, Alec Owens , Armando N. Perri , Marco Pezzella, Oleksiy Smola, Andrei Sokolov, Jingxin Zhang and Jonathan Tennyson ★

Department of Physics and Astronomy, University College London, Gower Street, WC1E 6BT London, UK

Accepted 2024 July 25. Received 2024 July 24; in original form 2024 May 14

ABSTRACT

A theoretical line list for $^{15}NH_3$ CoYuTe-15 is presented based on the empirical potential energy and *ab initio* dipole moments surfaces developed and used for the production of the ExoMol line list CoYuTe for $^{14}NH_3$. The ro-vibrational energy levels and wavefunctions are computed using the variational program TROVE. The line list ranges up to 10 000 cm^{-1} ($\lambda \geq 1$ μm) and contains 929 795 249 transitions between 1 269 961 states with $J \leq 30$. The line list should be applicable for temperatures up to ∼1000 K. To improve the accuracy of the line positions, a set of experimentally derived energy levels of $^{15}NH_3$ is produced using the MARVEL (Measured Active Rotation Vibration Energy Level) procedure. To this end, 37 experimental sources of the line positions of $^{15}NH_3$ available in the literature are collected, combined, and systematized to produce a self-consistent spectroscopic network of 21 095 $^{15}NH_3$ transitions covering 40 vibrational bands ranging up to 6818 cm^{-1} and resulting in 2777 energy term values. These MARVEL energies are then used to replace the theoretical values in the CoYuTe-15 line list and also complemented by pseudo-MARVEL energies obtained by an isotopologue extrapolation using the previously reported MARVEL energies of the $^{14}NH_3$ parent isotopologue of ammonia. A list of 53 856 high-resolution transitions between MARVEL states and theoretical intensities is provided in the HITRAN format. Comparison with the recent experimental spectra of $^{15}NH_3$ illustrate the potential of the line list for detections and as an efficient assistant in spectroscopic assignments. The line list is available from www.exomol.com.

Key words: molecular data – opacity – exoplanets – planets and satellites: atmospheres – stars: atmospheres – ISM: molecules.

1 INTRODUCTION

$^{15}NH_3$ has long been detected in interstellar molecular clouds (Schilke, Walmsley & Mauersberger 1991) where it is used as a tracer of the $^{15}N/^{14}N$ isotopic ratio (Charnley & Rodgers 2002; Gerin et al. 2009; Lis et al. 2010; Redaelli et al. 2023), planetary atmospheres (Fouchet et al. 2000, 2004; Fletcher et al. 2014) and the Earth atmosphere (Harper & Sharpe 1998), in meteorites (Pizzarello & Williams 2012), and in comets (Mumma & Charnley 2011). Very recently, Barrado et al. (2023) detected $^{15}NH_3$ in the atmosphere of a cool brown dwarf with with the Mid-Infrared Instrument of *JWST*.

This work is an update of our previous empirical room temperature line lists for $^{15}NH_3$ (Yurchenko 2015) as well line lists by Huang, Schwenke & Lee (2011a, b). Here, we present an extended variationally computed line list for $^{15}NH_3$ covering the rotational excitations up to $J = 30$ and the wavenumber range up to 10 000 cm^{-1} ($\lambda \geq 1$ μm). The line list is computed using the variational program TROVE (Yurchenko, Thiel & Jensen 2007) and the same computational set up used by Coles, Yurchenko & Tennyson (2019) to produce a hot line list for $^{14}NH_3$ called CoYuTe. The line list is then improved using a MARVELization procedure, where the theoretical energies of $^{15}NH_3$ are replaced by experimentally derived values obtained using the MARVEL (Measured Active Rotation Vibration Energy Level) procedure (Furtenbacher, Császár & Tennyson 2007; Tennyson et al. 2024a). To this end, an extensive set of experimental spectroscopic line positions of $^{15}NH_3$ has been collected from the literature (Good & Coles 1947; Chu & Freund 1973; Freund & Oka 1976; Karyakin et al. 1977; Jones 1978; Carlotti et al. 1980; Cohen 1980; Sasada 1980; Sattler & Worchesky 1981; Di Lonardo et al. 1982; Sasada et al. 1982; Shojachaghervand & Schwendeman 1983; Urban et al. 1983, 1985a, 1986; Urban, D'Cunha & Rao 1984; D'Cunha et al. 1985; Urban, Misra & Rao 1985b; Sasada & Schwendeman 1986; D'Cunha 1987; Devi et al. 1990; Moriwaki, Nakagawa & Shimizu 1991; Huttner, Frank & Nowicki 1992; Buffa et al. 1994; Schatz et al. 1994; Urban, Klee & Yamada 1994; Brown & Margolis 1996; Anders et al. 2000; Lees et al. 2006; Li, Lees & Xu 2007; Lees, Li & Xu 2008; Čermák et al. 2014; Földes et al. 2016; Canè et al. 2019, 2020) covering publication from 1947 (see Section 2), combined and organized to produce a self-consistent spectroscopic network and then used to produce experimentally derived MARVEL energies of $^{15}NH_3$. A new simplified and self-consistent reduced scheme to represent the ro-vibrational quantum numbers (QNs) of $^{15}NH_3$ is suggested consisting of six quantum labels.

In order to improve more calculated energies that do not have MARVEL counterparts, the so-called isotopologue interpolation (IE)

★ E-mails: s.yurchenko@ucl.ac.uk (SNY); j.tennyson@ucl.ac.uk (JT)

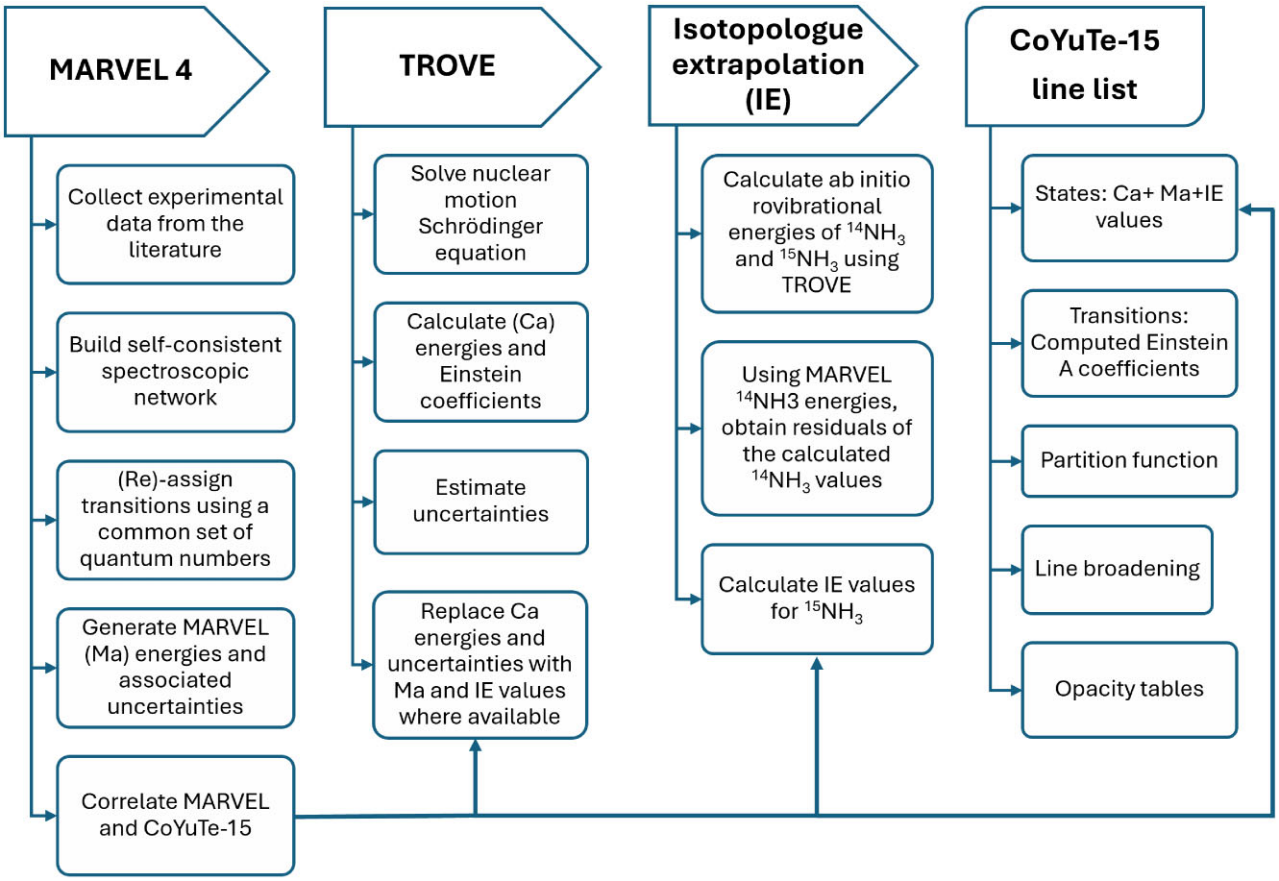

Figure 1. Line list construction steps.

procedure is employed. This procedure takes advantage of extensive experimental spectroscopic data available for the main isotopologue of a molecule and an observation that errors of the calculated ro-vibrational energies computed the same *ab initio* models are transferable between isotopologues of the same type (Polyansky et al. 2017).

The line list, comprising the ro-vibrational energies, lifetimes, Einstein A coefficients, partition functions as well as temperature- and pressure-dependent opacity tables is provided from the ExoMol data base at www.exomol.com. The line list is validated by comparing to HITRAN as well as to experimental spectra of $^{15}NH_3$.

For the construction of the line list for $^{15}NH_3$ we followed the following steps as outlined in the workflow diagram in Fig. 1: (i) compilation of experimental line positions of $^{15}NH_3$ from the literature and construction of experimentally derived energies using the MARVEL procedure (Furtenbacher et al. 2007); (ii) variational calculations of ro-vibrational energies and Einstein A coefficients using the program TROVE (Yurchenko et al. 2007); (iii) application of the isotopologue extrapolation (IE) technique; and (iv) production of the line list.

2 MARVEL PROCEDURE

2.1 The approach and input structure

The algorithm used for deriving empirical energy levels of $^{15}NH_3$ in this work is the MARVEL algorithm, developed by Furtenbacher and coworkers (Furtenbacher et al. 2007; Furtenbacher & Császár 2012a, b; Tóbiás et al. 2019; Tennyson et al. 2024a). The initial step in the MARVEL methodology involves compiling a data set of measured high-resolution spectroscopic transition frequencies commonly referred to as line positions.

The line positions used as an input for MARVEL need to feature QNs assigned to both upper and lower states, and to ensure uniformity, a consistent set of QNs is applied to all transitions. Furthermore, each line used is accompanied by its respective experimental uncertainty. The transitions are distinctly tagged, indicating the experimental source, and assigned a specific identifier within that source. Lastly, through the implementation of a weighted linear least-squares inversion procedure, MARVEL extracts a set of energy levels along with their corresponding uncertainties; here these uncertainties are actually recomputed using a bootstrap procedure (Tennyson et al. 2024a).

The goal is to create a cohesive network of energy levels, referred to as a spectroscopic network (Császár & Furtenbacher 2011; Császár et al. 2007; Furtenbacher et al. 2014). The transition uncertainties are systematically improved and incorrect lines are simultaneously removed from the data base. In more detail, a continuous assessment of the self-consistency of experimental transition frequencies is conducted. MARVEL identifies outliers, often caused by inaccurately assigned wavenumbers or during the transcription of the measured data into the transition list. In particular, transitions are flagged as invalid if the ratio between the optimal uncertainty and the original uncertainty exceeds a threshold of 100. These invalidated transitions are either corrected or annotated with a negative sign applied to their wavenumber values, to exclude them from further analysis by MARVEL.

Table 1. Correlation between the vibrational QNs and $\mathcal{D}_{3h}$(M) symmetries of ammonia ($n = 1, 2, 3, \ldots, m = 1, 2, 3, \ldots, \dagger = ', ''$). Here, $\dagger = '$ if K is even, and $\dagger = ''$ when K is odd.

	$n\nu_1$		$n\nu_2$		$n\nu_3^{l_3}$ or $n\nu_4^{l_4}$			$\lvert J, K, \tau_{\rm rot}\rangle$		
n		Γ	a/s	Γ	l_i	τ	Γ	K	$\tau_{\rm rot}$	$\Gamma_{\rm rot}$
any	0	A_1'	s	A_1'	0	0	A_1'	$3n$	0	$A_1^\dagger$
			a	A_2''	$3m$	0	A_1'	$3n$	1	$A_2^\dagger$
					$3m$	1	A_2'	$3n \pm 1$	0,1	$E^\dagger$
					$3m \pm 1$		E'			

Previously, the transition uncertainties were often manually increased in order to find the optimal set of uncertainties. However, the latest version of MARVEL offers a bootstrap method to iteratively determine the optimal energy level uncertainties (Tennyson et al. 2024a). With the bootstrap feature of MARVEL 4, the individual uncertainties of the MARVEL energies are determined to be suitable and reasonable. This is the method that was used in this work.

The MARVEL 4 online version (Tennyson et al. 2024a) which was used in the current study offers flexibility in handling transition energy units in comparison to earlier versions of MARVEL that were limited in only using cm^{-1}. MARVEL 4 online supports various units (cm^{-1}, Hz, kHz, MHz, GHz, and THz). To enable this expanded functionality, a segment file is included as an input, containing a compilation of the experimental source names with their respective units.

2.2 NH_3 quantum numbers

For the rotation and vibration states and motion of the pyramid like ammonia molecule with a feasible inversion mode, the $\mathcal{D}_{3h}$(M) molecular symmetry group is used. This group consists of six irreducible representations, A_1', A_2', E', A_1'', A_2'', and E'', referred to below also as symmetries. As for $^{14}NH_3$, the ro-vibrational states of $^{15}NH_3$ with A_1' and A_1'' symmetries do not exist due to the Pauli principle (Bunker & Jensen 1998).

2.3 Vibrational quantum numbers

There are four vibrational modes in ammonia, ν_1 (symmetric stretch), ν_2 (inversion), ν_3 (asymmetric stretch), and ν_4 (asymmetric bend), where ν_3 and ν_4 are doubly degenerate. The corresponding normal mode vibrational QNs are n_1, n_2, n_3, $l_3 n_4$, l_4, l, and s/a where $n_i \geq 0$ ($i = 1, 2, 3, 4$) are the vibrational quanta, l_3 and l_4 are the corresponding vibrational angular momentum QNs with $l = l_3 + l_4$ as the total vibrational angular momentum QN and the labels s and a are used to indicate if the inversion mode ν_2 is the symmetric or asymmetric, respectively. The values of l_i ($i = 3, 4$) satisfy

$$l_i = n_i, n_i - 2, n_i - 4, \ldots - (n_i - 4), -(n_i - 2), -n_i.$$

All excitations of ν_1 transform as A_1' in $\mathcal{D}_{3h}$(M). The symmetric property of the symmetric bending mode ν_2 upon the inversion (symmetric or asymmetric) provides the s/a labels to the full vibrational state. Inversion state of type $n_2\nu_2$ ($n_2 = 1, 2, 3, \ldots$) transform as A_1' (s) or A_2'' (a) in $\mathcal{D}_{3h}$(M). The values of l_i have a direct correlation with the symmetry of the corresponding contribution, based on the simple rule of multiple of three: states with $l_i \neq 3n$ have the symmetry E' forming degenerate pairs of the same values of $L_i = |l_i|$. States with $l_i = \pm 3n$ have symmetries A_1' or A_2' depending on the state parity $\tau = 0$ or 1, respectively, see Table 1.

The total vibrational symmetry $\Gamma_{\rm vib}$ is then the product of irreducible representations Γ_i from all four modes ν_i, after the associated reduction to the irreducible representation. For example, the state $\nu_1 + \nu_2$ ($n_1 = 1, n_2 = 1, n_3 = 0, n_4 = 0$) has the symmetry A_2'' as a direct symmetry product $A_1' \otimes A_2'' \otimes A_1' \otimes A_1'$, the state $3\nu_2 + \nu_4^{|l_4|=1}$ has the symmetry E' as the product $A_1' \otimes A_2'' \otimes E' \otimes A_1'$, while a more complex example $\nu_3^{|l_3|=1} + \nu_4^{|l_4|=2}$ spans three states: $(\nu_3^1 + \nu_4^2)^{|l|=3, A_1'}$, $(\nu_3^1 + \nu_4^2)^{|l|=3, A_2'}$, and $(\nu_3^1 + \nu_4^2)^{|l|=1, E'}$ as the result of the product (Bunker & Jensen 1998)

$$A_1' \otimes A_1' \otimes E' \otimes E' = A_1' \oplus A_2' \oplus E'.$$

The latter can be also interpreted as a result of the combination of the bending and stretching vibrational angular momenta $l_3 = \pm 1$ and $l_4 = \pm 2$, respectively:

$$l = l_3 + l_4 = \begin{cases} +1 + 2 = +3 & A_1'/A_2' \\ -1 - 2 = -3 & A_1'/A_2' \\ +1 - 2 = -1 & E' \\ -1 + 2 \ \ = 1 & E'. \end{cases} \quad (1)$$

Here, l as a total vibrational angular momentum is important to resolve the degeneracy of the three distinct components of the combinations l_3, l_4 in the $\nu_3^{|l_3|=1} + \nu_4^{|l_4|=2}$, which is necessary for the for the non-degenerate $l = \pm 3$ states. The same result, in principle, is achieved by using the total vibrational symmetry $\Gamma_{\rm vib}$, with $A_1^\dagger$ and $A_2^\dagger$ ($\dagger = '$ or $''$) to account for the two non-degenerate components of this combination. In fact, using symmetries is more physically sensible than the non-physical alternative with the defined signs $l = 3, -3$, but the former is more popular in experimental studies of ammonia and spherical tops in general.

2.4 Rotational quantum numbers

The rotational assignment follows the rigid rotor wavefunctions $|J, k, m\rangle$, where J is the total angular momentum QN, m is the projection of the total angular momentum on the laboratory fixed axis Z, and k is the projection of the total angular momentum on the molecular fixed axis z. Since m does not play any role in the classification of the rotational states in the absence of external fields, it is commonly omitted from the consideration.

In order to correlate to the molecular symmetry, the rigid rotor wavefunctions $|J, k, m\rangle$ are first combined into symmetric and asymmetric Wang-type functions $|J, K, \tau_{\rm rot}\rangle$ (Yurchenko et al. 2005)

$$|J, 0, \tau_{\rm rot}\rangle, \ \tau_{\rm rot} = J \bmod 2, \quad (2)$$

$$|J, K, \tau_{\rm rot}\rangle = \tfrac{1}{\sqrt{2}} \left[|J, |k|\rangle + (-1)^{J+K+\tau_{\rm rot}} |J, -|k|\rangle \right], \quad \tau_{\rm rot} = 0, 1, \quad (3)$$

where we introduced $K = |k|$ and $\tau_{\rm rot}$ to describe the parity of the rotational state and dropped m. The symmetries associated with different values of K and $\tau_{\rm rot}$ are explained in Table 1. Although

just two quantities, J and $K = |k|$ are sufficient for the description of the degenerate $E^\dagger$ states, when $K = 3n$, one more descriptor is required. In experimental studies, it is usually the sign of k that serves this purpose, which is however not well defined and often lead to ambiguity in descriptions of the experimental data from different sources. Here, we use the symmetries $\Gamma_{\rm rot} = A_1^\dagger$ and $A_2^\dagger$ to distinguish different states of the same $|K| = 3n$. This symmetry label is also used for states with $3n \pm 1$ when $\Gamma_{\rm rot} = E^\dagger$ for consistency.

2.5 Ro-vibrational quantum numbers

It should be noted that the absolute signs of l_3, l_4, or l are also ill-defined. Indeed, the positive and negative values of l (and also k, see below) contribute equally to the description of ro-vibrational states of symmetric tops giving rise to the so-called Wang 50/50 mixtures, see equation (3). The relative signs however do matter, which is the main reason for the signed values of ls commonly used in the spectroscopic analysis. Another reason is that the sign of l or k is effectively an additional quantum label allowing to distinguish states of the same absolute $|l|$ or $|k|$, even though they often lead to conflicting assignments of the same spectra from different experimental sources. Ammonia is characterized by its tunnelling motion which leads to inversion of the molecule and splitting of the levels into symmetric/antisymmetric combinations which we denote s/a. Depending on the choice of QNs, s/a can be redundant but still useful as the inversion splitting is a key motif of ammonia spectra.

Our QNs of choice are the following (unambiguous) quantities: J, n_1, n_2, n_3, n_4, $L_3 = |l_3|$, $L_4 = |l_4|$, $L = |l_3 + l_4|$ (i.e. absolute values of the corresponding vibrational angular momenta), $K = |k|$ (absolute value of the rotational QN), irreducible representations Γ, $\Gamma_{\rm vib}$, and $\Gamma_{\rm rot}$ of the total ro-vibrational state, as well as of the vibrational and rotational contributions and s/a. These QNs correspond closely to the ones recommended by Down et al. (2013) and used in the previous MARVEL studies of $^{14}NH_3$ (Al Derzi et al. 2015; Furtenbacher et al. 2020).

It is now becoming more and more common to use simplified, compact schemes for assigning ro-vibrational states where several QNs are combined into a single counting index. For example, in recent experimental studies of CH_4 (see Kefala et al. 2024), it is a counting ro-vibrational index within the same J, total symmetry Γ, and the polyad P. In the case of N_2O (Tennyson et al. 2024a), this is the index also within the same J, l (vibrational angular momentum), and polyad P. As will be discussed below, the vibrational QNs of ammonia become ambiguous at high vibrational excitations as they are coupled through rotational interactions, which mix vibrational states from the same and different polyads. Moreover, the coupling scheme between different degrees of freedom are complicated by the symmetry product rules making the usage of the vibrational QN less intuitive. We therefore decided to introduce a reduced QN scheme, with the minimal number of quantum indices that maintain the key aspects of the rotation-vibrational states. For ammonia, this is the description of the individual vibrational ($J = 0$) and rotational state contributions we would like to preserve. While the rotational part in the case of the symmetric top ammonia can be mainly described by the rotational QNs J and K, as a compact representation of the full set of the vibrational QNs $n_1, n_2, n_3^{l_3}, n_4^{l_4}, l, \Gamma_{\rm vib}$, we introduce a single vibrational index $N_{\rm s/a}$. This index counts all vibrational states, s or a, sorted according to their increased $J = 0$ energies:

$$N_{\rm s/a} = \left\{ n_1, n_2, n_3^{l_3}, n_4^{l_4}, l, \Gamma_{\rm vib}, {\rm s/a} \right\}. \tag{4}$$

Note that $N_{\rm s/a}$ counts s and a states separately, that is, the full inversion-vibrational description is according with $\{N_{\rm s/a}, {\rm s/a}\}$. Thus, our final set of the ro-vibrational QNs consists of the following six labels given by:

$$\mathrm{QN} = \left\{ J, \Gamma, N_{\rm s/a}, {\rm s/a}, K, \Gamma_{\rm rot} \right\}, \tag{5}$$

where we included the rotational symmetry $\Gamma_{\rm rot}$ in order to resolve the ambiguity occurring at $K = 3n$ for the non-degenerate $A_1^\dagger / A_2^\dagger$ components. While we replace the full vibrational description by $\{N_{\rm s/a}, {\rm s/a}\}$ in the MARVEL set for the sake of its compactness, the original eight-QN information is retained by providing a detailed correlation table between $\{N_{\rm s/a}, {\rm s/a}\}$ and $\left\{ n_1, n_2, n_3^{l_3}, n_4^{l_4}, l, \Gamma_{\rm vib}, {\rm s/a} \right\}$, which is given below in Section 4.1.

3 SELECTION RULES

The standard rigorous (electric dipole and single photon) selection rules in the case of ammonia spectra are

$$\Delta J = 0, \pm 1 \tag{6}$$

$$J' + J'' \neq 0, \tag{7}$$

$$A_2' \leftrightarrow A_2'' \quad \text{(ortho)}, \tag{8}$$

$$E' \leftrightarrow E'' \quad \text{(para)}, \tag{9}$$

where A_1' and A_1'' do not exist due to the Pauli principle (the corresponding nuclear statistical weights are zero). Since the parity ($'$ or $''$) changes through a electric dipole, single photon transition, which is also directly correlated with the s/a characteristics, one can also obtain the following rigorous rules for s/a:

ΔK even : s $\leftrightarrow$ a
ΔK odd : s $\leftrightarrow$ s, a $\leftrightarrow$ a.

This is because K flips the parity of the vibrational states when K is odd. For the two-photon transitions, the selection rules are

$$\Delta J = 0, \pm 1, \pm 2, \tag{10}$$

$$J' + J'' \neq 0, \tag{11}$$

$$A_2^\dagger \leftrightarrow A_2^\dagger, \tag{12}$$

$$E^\dagger \leftrightarrow E^\dagger. \tag{13}$$

A number of two-photon spectra have been recorded experimentally (Freund & Oka 1976; Jones 1978; Shojachaghervand & Schwendeman 1983; Anders et al. 2000), but no transitions with $\Delta J = \pm 2$ have been observed; these transitions are allowed but expected to be too weak to readily observable (Shojachaghervand & Schwendeman 1983).

Most of the experimental data collected in this work are from single-photon electric dipole spectra. There are no transitions between para and ortho states and therefore a single estimated ortho–para transition frequency (magic number) was required to connect the ortho- and para networks (see below).

Ammonia has a rather strong $\Delta K = 0$ propensity rule which can cause networks to fragment and problems with effective Hamiltonian representations, see Furtenbacher et al. (2020) for a discussion of this issue. For the current data set, half of transitions (49 per cent) are with $\Delta K = 0$, 37 per cent with $\Delta K = 1$, 8 per cent with $\Delta K = 2$ and only 6 per cent is for all other transitions $\Delta K > 2$.

Table 2. Description of the MARVEL data of the experimental transitions of $^{15}NH_3$ used in this work.

Source	Units	Range	A/V	unc	s/d	Bands
47GoCo	MHz	20272.04−25323.51	0.02000	20/20	s	rot-inv
73ChFr	MHz	175054.90−175054.90	0.50000	1/1	s	rot-inv
76FrOk	cm^{-1}	921.75−987.63	0.00020	19/19	d	$\nu_2 - \nu_2$
77KaKrPa	MHz	430038.30−430038.30	0.20000	1/1	s	$\nu_2 - \nu_2$
78Jones	cm^{-1}	888.04−1090.97	0.00020	11/11	s/d	ν_2
80CaTrVe	cm^{-1}	38.92−276.87	0.00319	195/194	s	rot-inv
80Cohen	MHz	21904.29−55581.98	0.02009	45/41	s	$\nu_4 - \nu_4$
80Sasada	MHz	8180.56−44160.66	0.09922	115/114	s	rot-inv
81SaWo	cm^{-1}	926.84−1082.12	0.00020	14/14	s	ν_2
82DiFuTrMi	cm^{-1}	511.11−13017.41	0.00575	1926/1853	s	ν_2, $2\nu_2$, $3\nu_2$, ν_4, $\nu_2 + \nu_4$
82SaHaAmSh	cm^{-1}	697.00−1838.71	0.05000	775/385	s	ν_4, $2\nu_2$
83ShSc	cm^{-1}	916.75−1091.54	0.00020	120/118	d	ν_2
83UrPaBeKr	cm^{-1}	18.31−1098.02	0.00061	207/205	s	ν_2, $\nu_2 - \nu_2$
84UrDCRa	cm^{-1}	809.44−1026.49	0.00200	5/5	s	ν_2
85DCUrRa	cm^{-1}	697.74−1225.72	0.00050	499/499	s	ν_2
85UrDCRaPa	cm^{-1}	1129.21−2100.01	0.00493	807/791	s	$2\nu_2$, ν_4
85UrMiRa	cm^{-1}	3163.21−4495.55	0.00922	484/483	s	$\nu_1 + \nu_2$, $\nu_1 + \nu_2 - \nu_2$
86SaSc	cm^{-1}	720.71−1169.02	0.01092	150/150	s	$2\nu_2$–ν_2
86UrDCMa	cm^{-1}	533.67−1328.74	0.00505	433/411	s	ν_2
87DCunha	cm^{-1}	695.26−1179.20	0.00260	199/196	s	$2\nu_2$–ν_2
90DeRaPrUr	cm^{-1}	1494.62−1533.29	0.02000	33/0	s	ν_4
91MoNaSh	cm^{-1}	15237.32−15535.90	0.00500	129/0	s	$5\nu_1$
92HuFrNo	MHz	30590.99−54321.94	0.02927	26/25	s	$\nu_4 - \nu_4$
94BuLuTaMa	KHz	18871541.30−23421979.50	1.70000	5/5	s	rot-inv
94ScReFuIz	cm^{-1}	33.14−1085.15	0.05150	60/38	s	$\nu_2 - \nu_2$
94UrKlYa	cm^{-1}	19.08−119.53	0.00007	33/33	s	rot-inv
96BrMa	cm^{-1}	4944.50−5179.79	0.00030	129/124	s	$\nu_3 + \nu_4$
00AnJoLeSa	cm^{-1}	3328.20−3333.51	0.00233	56/55	s	ν_1
00AnJoLeSa(IR)	cm^{-1}	3327.62−3334.11	0.00006	71/71	d	ν_1
06LeLiLiXu	cm^{-1}	6372.64−6777.71	0.02000	272/268	s	$\nu_1 + \nu_3$
07LiLeXu	cm^{-1}	6412.16−6687.72	0.00381	96/95	s	$\nu_1 + 2\nu_4$
08LeLiXu	cm^{-1}	6446.10−6817.69	0.04387	224/219	s	$\nu_3 + 2\nu_4$, $\nu_1 + \nu_3$, $2\nu_1$, $\nu_1 + 2\nu_4$
14CeHoVeCa	cm^{-1}	4275.01−4339.22	0.00200	183/179	s	ν_1, $\nu_2 + \nu_3$, $2\nu_2 + \nu_3$-ν_2
16FoVaRiHe	cm^{-1}	6300.39−6790.79	0.00600	590/522	s	$\nu_1 + \nu_3$
19CaLoFuTa	cm^{-1}	5.84−2126.90	0.00076	7449/7428	s	$\nu_4 - \nu_4$
19CaLoFuTa(MHz)	MHz	21904.29−168831.50	0.02380	69/66	s	$\nu_2 - \nu_2$, $2\nu_2 - 2\nu_2$, $\nu_4 - \nu_4$ (and between)
20CaLoFu	cm^{-1}	67.06−3076.22	0.00111	5770/5447	s	$\nu_2 + \nu_4$, $3\nu_2$
MAGIC	cm^{-1}	15.39−2175.89	0.00010	2/2	s	rot-inv

Notes. A/V are the numbers of the available and validated transitions, respectively; unc is mean uncertainty, in the units of the original source; the label s/d indicate single/double photon transitions.

4 EXPERIMENTAL DATA SOURCES

In the following, the existing experimental sources containing transition frequencies of $^{15}NH_3$ are reviewed. Detailed statistics, including the number of lines considered and validated, are presented in Table 2.

47GoCo (Good & Coles 1947). 20 mm (kHz) wave inversion transitions $Q(J)$ with uncertainty 0.02 kHz.

73ChFr (Chu & Freund 1973). A millimetre wave rotation-inversion line $R(1)$ in the ν_2 hot band with uncertainty 0.5 MHz; QNs were taken from 83UrPaBeKr.

76FrOk (Freund & Oka 1976). Two-photon (forbidden) transitions in the ν_2 band. Uncertainty provided.

77KaKrPa (Karyakin et al. 1977). One inversion line, $\nu_2 - \nu_2$ hot band.

78Jones (Jones 1978). Eleven infrared transitions of the ν_2 band; a/s labels of IR for some transitions had to be swapped to match other data. 78Jones also report two-photon transitions of $^{15}NH_3$ with incomplete (or confusing) assignment which we could not match to the data from other sources and excluded.

80CaTrVe (Carlotti et al. 1980). Rotation-inversion spectrum; the stated uncertainties are 0.01 cm^{-1} for blended lines or 0.001 cm^{-1}, otherwise.

80Cohen (Cohen 1980). Inversion band within ν_4.

80Sasada (Sasada 1980) Microwave inversion band. Uncertainty of 0.1 MHz was assumed.

81SaWo (Sattler & Worchesky 1981). The ν_2 band. Here, it was important to include the vibrational symmetry into the state assignment for states with $K = 3$ due to the degeneracy associated with states of A_1/A_2. We used TROVE QNs and energies for reconstructing the state symmetries for all states.

82DiFuTrMi (Di Lonardo et al. 1982). The ν_2, $2\nu_2$, $3\nu_2$, ν_4, and $\nu_2 + \nu_4$ bands. Stated uncertainty = 0.0001 cm^{-1}, which we doubled for blended lines. 1883 transitions were validated out of 1926. Some l's were changed to match more recent experimental assignment (19CaLoFaTa) if the upper state energies in the associated combination differences (CDs) matched. The upper values of 's/a' were assigned using the rule of $(K' - K'')$ should odd/even for 's/a' to change/not to change.

82SaHaAmSh (Sasada et al. 1982). The ν_4 and $2\nu_2$ bands. Some of the $2\nu_2/\nu_4$ assignments were swapped when matching to other sources. The uncertainties were set to 0.05 cm^{-1}, but the data appear to be of lower quality and inconsistent with this uncertainty; they conflict with many other observations leading to large differences in CDs, significantly higher this the uncertainty. Only 385 out of 775 transitions could be validated.

83ShSc (Shojachaghervand & Schwendeman 1983). The ν_2 band, 120 two-photon forbidden transitions; uncertainty was stated in the paper of 0.0002 cm^{-1}.

83UrPaBeKr (Urban et al. 1983). The ν_2 and $\nu_2 - \nu_2$ bands. All negative k were changed to positive $K = |k|$ to make consistent with out convention. The uncertainty values are stated as 0.001–0.00003 cm^{-1}.

84UrDCRa (Urban et al. 1984). Five forbidden transitions in the ν_2 band.

85DcUrRa (D'Cunha et al. 1985). The ν_2 band. Uncertainties are provided.

85UrDCRaPa (Urban et al. 1985a). Bands $2\nu_2$ and ν_4. Accurate ground state (g.s.) energies and ν_2 energies are reported, which were them used in the CDs calculations. We changed some ls to match more recent data of Canè et al. (2019) based on the CDs (i.e. on the match of the upper state energies). Some of the $2\nu_2$ states were reassigned to ν_4 using TROVE matches and to agree with CDs from other sources. Many of the uncertainties were increased to 0.1 cm^{-1} based on the CDs analysis. Only eight transitions could not be validated out of 807.

85UrMiRa (Urban et al. 1985b). The overtone $\nu_1 + \nu_2$ and hot $\nu_1 + \nu_2 - \nu_2$ bands. Uncertainties are provided.

86SaSc (Sasada & Schwendeman 1986). Hot band $2\nu_2$–ν_2. Uncertainties are provided.

86UrDCMa (Urban et al. 1986). The ν_2 band. The upper state s/a were defined using the usual rule for the single-photon transitions. Uncertanties are provided.

87DCunha (D'Cunha 1987). Hot band $2\nu_2$–ν_2. Uncertainties are provided and claimed to be better than 0.002 cm^{-1}.

90DeRaPrUr (Devi et al. 1990). The ν_4 band. Mainly intensities are reported alongside line frequencies. It is not clear if the line frequencies are experimental or theoretical. Excluded.

91MoNakShi (Moriwaki et al. 1991). Reports transitions in the region of the $5\nu_1$ band, but no specific sub-band assignment is given. The assignments are very limited and we could not make them work so this data set was excluded.

92HuFrNo (Huttner et al. 1992). The 26 hot band $\nu_4 - \nu_4$ transitions; uncertainties 0.02–0.05 MHz as provided.

94BuLuTaMa (Buffa et al. 1994). Five pure rotational lines in kHz.

94ScReFuIz (Schatz et al. 1994). The $\nu_2 - \nu_2$ hot band: Far-infrared emission lines, produced by both inversion (single-photon) and Raman (two-photon) processes. Large uncertainties of 0.05 cm^{-1} were assumed due to two decimal places given. Some are pure rotational within g.s. and some are hot within ν_2. Not all lines could be validated.

94UrKlYa (Urban et al. 1994). Far-infrared g.s. rotation-inversion transitions. Uncertainty is stated to be 0.000003 cm^{-1}.

96BrMa (Brown & Margolis 1996). 5294 cm^{-1} region containing $\nu_3 + \nu_4$ band. All $l' = 1/l' = -1$ (non-physical for $\nu_3 + \nu_4$) were reassigned to $l' = 2/l' = -2$. 96BrMa.22 excluded because it disagrees with 96BrMa.18. Reported uncertainty 0.0003 cm^{-1} in the paper.

00AnJoLeSa and 00AnJoLeSa(IR) form (Anders et al. 2000). 00AnJoLeSa contains ν_1 Raman (two-photon forbidden) transitions; and 00AnJoLeSa.72 is from a non-physical state ($J = 0$, A_1 g.s.) and was excluded. 00AnJoLeSa(IR) contains single photon (IR) transitions. We separated these transitions into two parts to facilitate handling these two distinct data sets.

06LeLiLiXu (Lees et al. 2006). The $\nu_1 + \nu_3$ band. Some transitions were reassigned to $2\nu_1$ and $(\nu_3 + 2\nu_4)^1$ to match TROVE.

07LiLeXu (Li et al. 2007). The $\nu_1 + 2\nu_4$ band, transitions, and term values.

08LeLiXu (Lees et al. 2008). Reported transitions from the 1.5 μm region containing the $\nu_3 + 2\nu_4$ band. Some lines were changed to $\nu_1 + \nu_3$, $2\nu_1$, and $\nu_1 + 2\nu_4$ based on the CDs analysis.

14CeHoVeCa (Čermák et al. 2014). Bands ν_1, $\nu_2 + \nu_3$, and $2\nu_2 + \nu_3 - \nu_2$ from the 2.3 μm region. All but four transitions were validated (179 out of 183).

16FoVaRiHe (Földes et al. 2016). Transitions from the $\nu_1 + \nu_3$ band are reported but without specific assignment of the individual bands, that is, all transitions are initially assigned to $\nu_1 + \nu_3$. Some of the lines were vibrationally reassigned by a combined CD analysis with the assigned data from 08LeLiXu (Lees et al. 2008) covering the same upper states. Many lines even with multiple CDs could not be validated and were excluded as they lead to upper energies which conflict with those given by other sources and our TROVE calculations.

19CaLoFuTa(MHz) and 19CaLoFuTa, from (Canè et al. 2019). 19CaLoFuTa(MHz) contains $\nu_4 - \nu_4$ data in MHz, while 19CaLoFuTa reports transitions from the $\nu_2 - \nu_2$, $2\nu_2 - 2\nu_2$, and $\nu_4 - \nu_4$ bands are in cm^{-1}. We separate 19CaLoFuTa (MHz) from 19CaLoFuTa (cm^{-1}) because of the structure of the MARVEL4 input requiring the data in the original units. Only 10 transitions out of 7563 could not be validated.

20CaLoFu (Canè et al. 2020). This a second largest source reporting 5770 transitions from the bands $\nu_2 + \nu_4$ and $3\nu_2$. About 250 transitions could not be validated because of conflicts with the experimental data from other sources as well as unusually large differences with our theoretical (TROVE) estimates. Among those cases, the most unexpected disagreement was found for five $\nu_2 + \nu_4$ energy levels of 20CaLoFu ($J = 5, 6, 7, 8$), all supported by multiple (up to 9) transitions with CDs within about 0.02 cm^{-1}, that conflicted with the corresponding theoretical energies of TROVE by more than 8–16 cm^{-1}. Considering that in all other cases, TROVE energies agree with MARVEL to much better than 1 cm^{-1}, these five groups of transitions were first considered as suspicious and then treated as experimental outliers, possibly caused by impurities present in experimental spectra of Canè et al. (2020). Moreover, in all these case, we could find at least one transition from 82SaHaAmSh from the same levels that agreed with TROVE within 0.01 cm^{-1}. An example of such suspected false CDs is illustrated in Table 3, where we show eight transitions from 20CaLoFu with a common upper state $J = 5$, $K' = 1$, a, A_2', $\Gamma_{\rm rot=}E''$, and $N = 5$ ($\nu_2 + \nu_4$). The corresponding combination seemingly agree with each other leading to an upper energy term value of 2874.127 cm^{-1}. This prediction is however very far from the TROVE value of 2882.4683 cm^{-1}, which does not seem to be unrealistic considering the generally very good agreement for most of the MARVEL energies (94 per cent are within 0.1 cm^{-1}), see below, including the $\nu_2 + \nu_4$ band. Moreover, the experimental data set 82DiFuTrMi (Di Lonardo et al. 1982) also contains a transition to this state with the upper state energy of 2882.4596 cm^{-1}, which is an excellent agreement with the TROVE prediction, see Table 3. We have encountered at least four similar cases with a large number of CDs (∼8), all for $\nu_2 + \nu_4$ with $J = 5, 6, 7, 8$ from 20CaLoFu (Canè et al. 2020), with large differences from TROVE (8–16 cm^{-1}) and in every case with an alternative, single transition from 82DiFuTrMi (Di Lonardo et al. 1982) in an excellent agreement with TROVE. Although

Table 3. Example of CDs from 20CaLoFu (Canè et al. 2020) conflicted with the TROVE prediction of the upper state energy of 2882.4683 cm^{-1} as well as of the value from the single line 82DiFuTrMi (Di Lonardo et al. 1982), 2882.459601 cm^{-1}, which agree with each other.

$\tilde{\nu}$ (cm^{-1})	unc (cm^{-1})	J''	K''	a/s''	Γ''	Γ''_{rot}	N	Line	$\tilde{E}'$ (cm^{-1})	$\tilde{E}''$ (cm^{-1})
134.74608	0.0004	4	1	s	A_2''	E''	6	20CaLoFu.112	2874.127322	2739.38124
1046.35599	0.0060	4	1	s	A_2''	E''	4	20CaLoFu.2818	2874.127558	1827.77157
809.85126	0.0006	4	0	a	A_2''	A_1'	3	20CaLoFu.2006	2874.127853	2064.27659
1497.88856	0.0006	6	0	a	A_2''	A_1'	2	20CaLoFu.3924	2874.128003	1376.23944
2458.29564	0.0006	6	0	a	A_2''	A_1'	1	20CaLoFu.5059	2874.128241	415.83260
597.3536	0.0006	6	0	a	A_2''	A_1'	3	20CaLoFu.1254	2874.128864	2276.77526
952.45873	0.0006	5	1	s	A_2''	E''	4	20CaLoFu.2585	2874.129251	1921.67052
1714.09336	0.0006	4	0	a	A_2''	A_1'	2	20CaLoFu.4453	2874.129451	1160.03609
2466.627	0.0040	6	0	a	A_2''	A_1'	1	82DiFuTrMi.1633	2882.459601	415.83260

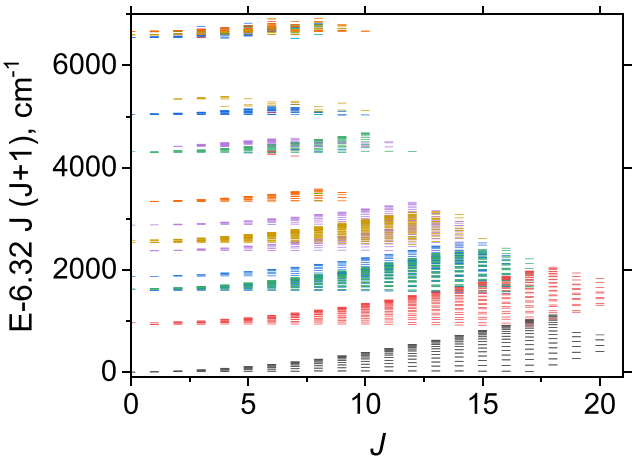

Figure 2. MARVEL reduced energy term values of $^{15}NH_3$ with different vibrational bands forming a clear pattern.

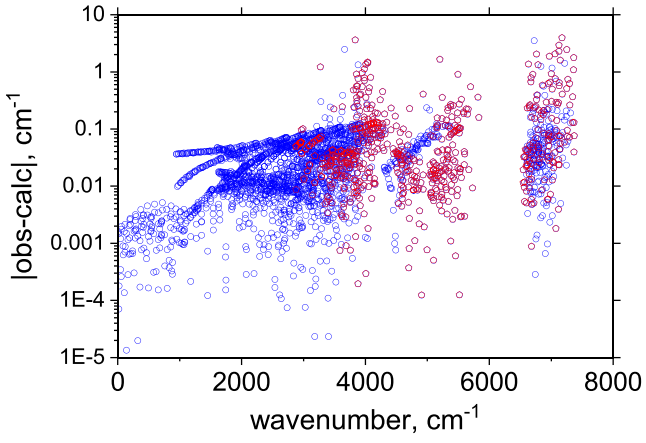

Figure 3. Obs.–calc. (MARVEL-CoYuTe-15) as a function of the energy term value. The diamonds indicate MARVEL energies defined by one or single transitions only.

this is not obvious, but we decided to trust the TROVE and 82DiFuTrMi predictions in those cases and excluded the corresponding transitions from MARVEL.

4.1 MARVEL

By the MARVEL definition, MARVEL energy of the lowest state is set to zero, which in case of $^{15}NH_3$ is $J = 0$, $K = 0$, a, A_2'' ($0,0,0^0, 0^0$), that is, the upper, asymmetric inversion component of the g.s. state, with the symmetric component $J = 0$, $K = 0$, s, and A_2' ($0,0,0^0, 0^0$) non-existent due to the nuclear spin statistics. Because of this effect, the inversion splitting of ammonia $^{15}NH_3$ cannot be observed experimentally and is not present in our MARVEL set.

In order to connect the ortho- and para networks, we used a 'MAGIC' number (i.e. not experimental) as an energy difference between lowest (g.s.) energy levels of para- and ortho states, $J = 1$, $K = 1$, s (E'') and $J = 0$, $K = 0$, a (A_2''), respectively, taken from the term values list by Urban et al. (1985a): $\Delta\tilde{E} = 15.391430\,cm^{-1}$. Fig. 2 shows the MARVEL energies of $^{15}NH_3$.

4.2 MARVEL and correlation between experiment and theory

The experimental transitions in our list all originate from six lower states, g.s., ν_2, $2\nu_2$, ν_4, $2\nu_4$, and $\nu_2 + \nu_4$, which correspond to $N_{s/a} =$ 1, 2, 3, 4, 5, and 6, respectively. We started by building CDs for experimental transitions originating from g.s. and ν_2, where we could take advantage of the existing energy term values from Urban et al. (1985a). By applying these term values to the transitions from Di Lonardo et al. (1982); Sasada et al. (1982); Urban et al. (1985a); Sasada & Schwendeman (1986); D'Cunha (1987); Devi et al. (1990); Canè et al. (2019, 2020), the CDs for the upper state ν_4, $2\nu_2$, $2\nu_4$, and $\nu_2 + \nu_4$ could be constructed and the corresponding energies compared. This procedure helped identify and correct possible misassignments of many upper states. In turn, the corresponding term values could be used to construct CDs for all other hot bands originated from these states.

To facilitate this procedure, the CoYuTe-15 line list was extensively used. Our ultimate goal is to use the experimentally derived MARVEL energies in place of the theoretical values where available. To this end, the MARVEL energies need to be correlated to the calculated TROVE energies. Being able to compare the two sets of data to each other helps both ways, to establish the quality of the variational calculations but also resolve potential problems in the MARVEL set.

Owing to the high quality of the underlying empirical potential energy surface (PES) of NH_3, the theoretical ro-vibrational term values and associated CDs were of reasonably high quality, see Fig. 3. To help match experiment and theory, the signs of different values of l and k, and sometimes of l_3 and l_4 in the experimental sources had to be reassigned to make them consistent between different experimental data. In many case, the associated (non-rigorous) QN had to be modified, including the vibrational ones, n_1, n_2, n_3, and n_4. However, the rigorous QNs J and symmetry were not altered. In order to correlate to TROVE, some TROVE quantum numbers had

Table 4. Vibrational ($J = 0$) energy term values $\tilde{E}$, experimental QNs (n_1, n_2, $n_3^{l_3}$, $n_4^{l_4}$, l, s/a), and their mapping to the labels $N_{s/a}$ and Γ_{vib} for all vibrational state used in our MARVEL set for $^{15}NH_3$.

$N_{s/a}$	$\tilde{E}^{(s)}$ (cm^{-1})	$\tilde{E}^{(a)}$ (cm^{-1})	n_1	n_2	n_3	l_3	n_4	l_4	l	Γ_{vib}
1	0.0000	0.759258	0	0	0	0	0	0	0	A_1'
2	928.4200	962.884440	0	1	0	0	0	0	0	A_1'
3	1591.1451	1870.839271	0	2	0	0	0	0	0	A_1'
4	1623.1601	1624.223193	0	0	0	0	1	1	1	E'
5	2369.3052	2876.114293	0	3	0	0	0	0	0	A_1'
6	2533.3162	2577.600578	0	1	0	0	1	1	−1	E'
9	3233.9370		1	0	0	0	0	0	0	E'
10	3333.3021	3334.268304	1	0	0	0	0	0	0	A_1'
12	3438.6186		1	0	0	0	0	0	0	A_1'
14		4161.664679	0	1	0	0	2	0	0	A_2''
15	4125.4594	4181.129616	0	1	0	0	2	2	2	E'
16	4288.0489	4312.285044	1	1	0	0	0	0	0	A_1'
17	4403.6103	4421.482245	0	1	1	1	0	0	1	E'
19	4742.9544		0	0	1	1	1	1	2	A_1'
20		5095.012196	0	0	1	1	1	1	2	E''
21	4790.9936	4793.138030	0	0	1	1	1	1	2	E'
26	5040.5521	5041.175789	0	0	1	1	1	1	2	A_2'
27	5041.2057	5041.819217	0	0	1	1	1	1	2	E'
30	5129.3266	5333.267022	0	2	1	1	0	0	1	E'
41		6702.902353	0	0	1	−1	2	2	1	A_2''
43	6294.3854	6660.407789	1	0	0	0	2	2	2	E'
45		6693.154085	0	0	2	0	3	3	1	A_2''
48		6364.423717	0	0	0	0	4	4	2	E''
50	6511.6301	6513.176308	2	0	0	0	0	0	0	A_1'
51	6546.9982	6548.468141	1	0	0	0	2	2	2	E'
52	6570.4264		1	0	2	0	0	1	1	E'
53	6595.0789	6595.961735	2	0	0	0	0	0	0	A_1'
54	6596.5904	6597.461983	1	0	1	1	0	0	1	E'
55	6636.6412		0	0	1	−1	2	2	1	A_2'
56	6637.6712	6638.904945	0	0	1	1	2	2	1	A_1'
57	6651.4442	6650.418625	0	0	2	2	1	1	1	E''
58	6664.6067	6665.278000	0	0	1	−1	2	2	1	E'
59	6681.2824		0	0	1	1	2	−2	−1	A_1'
60	6692.8086		1	0	1	1	0	0	1	A_2'
61	6698.1314		0	0	1	1	2	−2	−1	E'
62	6705.3820		1	0	1	1	0	0	1	E'
63	6709.1670		0	2	1	1	1	1	1	A_1'
66	6833.9506	6834.678719	1	0	1	1	0	0	1	E'

Table 5. Extract from the MARVEL transition file. The MARVEL frequency wavenumber $\tilde{\nu}$ and uncertainties are in cm^{-1}. The mapping between the compact vibrational index $N_{s/a}$ and the full set of the vibrational QNs, see equation (4), is illustrated in Table 4. There are two uncertainty columns to allow the input uncertainty to be updated while retaining the original uncertainty of the source.

$\tilde{\nu}$	unc. (cm^{-1})	unc. (cm^{-1})	Quantum 'numbers' of upper states						Quantum 'numbers' of lower states						Source
			J'	K'	s/a'	Γ'	Γ'_{rot}	$N'_{s/a}$	J''	K''	s/a''	Γ''	Γ''_{rot}	$N''_{s/a}$	
5158.7121	0.0003	0.0003	6	1	s	A_2''	E'	27	5	0	s	A_2'	A_2'	1	96BrMa.128
5179.7856	0.0003	0.0003	7	1	a	A_2'	E'	27	6	0	a	A_2''	A_1'	1	96BrMa.129
19.083628	0.000003	0.000003	1	0	s	A_2'	A_2'	1	0	0	a	A_2''	A_1'	1	94UrKlYa.1
38.913812	0.00006	0.00006	2	1	s	E'	E'	1	1	1	a	E'	E'	1	94UrKlYa.2
40.390961	0.00004	0.00004	2	0	a	A_2''	A_1'	1	1	0	s	A_2'	A_2'	1	94UrKlYa.3
40.403877	0.00004	0.00004	2	1	a	E'	E'	1	1	1	s	E'	E'	1	94UrKlYa.4
58.713871	0.00004	0.00004	3	0	s	A_2'	A_2'	1	2	0	a	A_2''	A_1'	1	94UrKlYa.5
58.7166	0.00006	0.00006	3	1	s	E'	E'	1	2	1	a	E'	E'	1	94UrKlYa.6

to be modified to make them unambiguous and consistent with the experiment.

As part of the process, a set of term values was compiled to be used as lower states for the experimental set of $^{15}NH_3$ we collected based on a mixture of the experimentally derived term values of 85UrCrPa (g.s. and ν_2) and TROVE term values. We then were able to correlate all the upper and lower states from the experimental transitions to the TROVE ro-vibrational states and thus use the TROVE QNs as an independent self-consistent set of assignments. This procedure helped correlate the experimental transitions from different sources featuring the same states, correct assignments, identify, and exclude outliers.

Once the full correlation was constructed, it was then possible to replace the experimental QNs with our MARVEL set of six QNs in equation (5). This set is based on the collective vibrational QN $N_{s/a}$, which is defined as a counting index of the vibrational

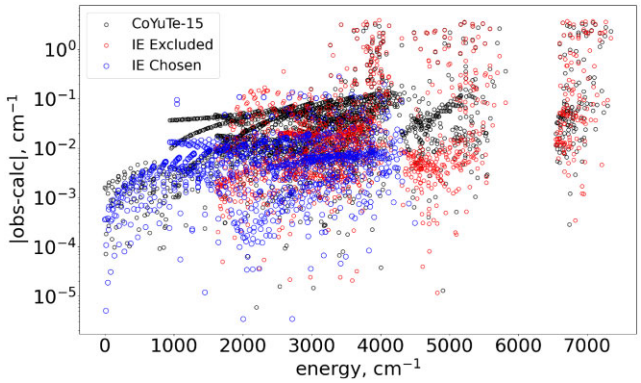

Figure 4. Absolute values of residuals $|\tilde{E}^{\rm obs.} - \tilde{E}^{\rm calc.}|$ (|obs − calc|) between the CoYuTe-15 energies and the MARVEL energies alongside the IE residuals as a function of the energy term value. IE levels from bands selected for substitution are highlighted separately.

Table 6. IE and CoYuTe-15 root-mean-squared obs. − calc. of $^{15}NH_3$ bands chosen for IE substitution.

N	a/s	State	IE (cm^{-1})	CoYuTe-15 (cm^{-1})
1	s	g.s.	0.019505	0.021751
1	a	g.s.	0.018846	0.019437
2	s	ν_2	0.023396	0.064547
2	a	ν_2	0.022278	0.065662
4	a	$2\nu_2$	0.027318	0.059184
5	s	$3\nu_2$	0.018277	0.035313
6	a	$3\nu_2$	0.024460	0.058929

($J = 0$, s or a) energy term values, including the non-existing A_1' and A_1'' states. The latter are also important as they play the role of the 'band centres' for the ro-vibrational term values or transition frequencies. The correlation between $N_{\rm s/a}$ and the vibrational QNs $\left\{n_1, n_2, n_3^{l_3}, n_4^{l_4}, l, \Gamma_{\rm vib}, {\rm s/a}\right\}$ is illustrated in Table 4 for all vibrational states from our MARVEL data. The full correlation table is given as Supporting Information. We used the theoretical, CoYuTe-15, term values to establish the correlation between the vibration-inversion states and $\{N_{\rm s/a}, {\rm s/a}\}$. Being theoretical, our quantum label $N_{\rm s/a}$ has the caveat of depending on the order of the CoYuTe-15 energies and is thus affected by its quality, especially at higher excitations.

As an illustration of the MARVEL data structure, in Table 5 we provide an extract from the main MARVEL data set. In order to help the users with our compact assignment scheme, especially with the new counting index $N_{\rm s/a}$, in the Supporting Information we also provide (i) the original CoYuTe-15 vibrational term values $N_{\rm s/a}$ is based on, accompanied by the mapping with the experimental QNs from equation (4) (see Table 4); and (ii) the experimental transitions using the native QNs (subject to some corrections for internal consistency).

5 LINE LIST PRODUCTION

5.1 TROVE calculations

The CoYuTe-15 line list has been produced using the variational code TROVE (Yurchenko et al. 2007) with the spectroscopic model from Coles et al. (2019) developed and used for the CoYuTe line list for $^{14}NH_3$, where we switched to the (atomic) masses $m_{\rm N} = 15.000108898$ Da and $m_H = 1.007825032$ Da. This spectroscopic model consists of an empirical PES fitted by Coles et al. (2018) and an *ab initio* electric dipole moment surface (DMS) from Yurchenko et al. (2009). For the details of the computational set up see Coles et al. (2019), which we only briefly describe here.

Table 7. Uncertainties $\delta_{\rm IE}$ used for IE levels based on the state, J and the uncertainty δ_{14} of the corresponding MARVEL level for the $^{14}NH_3$ isotopologue.

State	a/s	J	δ_{14} (cm^{-1})	$\delta_{\rm IE}$ (cm^{-1})
g.s.	s	≤ 10	$\leq 1.2 \times 10^{-3}$	10^{-2}
		> 10	$\leq 1.2 \times 10^{-3}$	10^{-1}
		> 10	$> 1.2 \times 10^{-3}$	2×10^{-1}
g.s.	a	≤ 10	$\leq 10^{-3}$	10^{-2}
		> 10	$\leq 10^{-3}$	10^{-1}
		> 10	$> 10^{-3}$	2×10^{-1}
ν_2	s	N/A	$\leq 1.2 \times 10^{-3}$	10^{-1}
		N/A	$> 1.2 \times 10^{-3}$	2×10^{-1}
ν_2	a	≤ 10	$\leq 10^{-3}$	10^{-2}
		> 10	$\leq 10^{-3}$	10^{-1}
		> 10	$> 10^{-3}$	2×10^{-1}
$2\nu_2$	a	≤ 10	N/A	10^{-2}
		> 10	N/A	10^{-1}
$3\nu_2$	s	N/A	$\leq 10^{-3}$	10^{-1}
		N/A	$> 10^{-3}$	2×10^{-1}
$3\nu_2$	a	N/A	$\leq 7.5 \times 10^{-4}$	10^{-1}
		N/A	$> 7.5 \times 10^{-4}$	2×10^{-1}

The kinetic energy operator was expanded in terms of five linearized coordinates $\xi_i^{\rm lin}$, $i = 1, \ldots, 5$ around a non-rigid (inversion) frame on a equidistant grid of 1000 points covering the umbrella coordinate δ from -55° to 55°. The umbrella coordinate is defined as an angle between any of the N-H$_i$ modes and their trisector (see Yurchenko 2023). The five coordinates $\xi_i^{\rm lin}$ are constructed from the following valence coordinates: the three bond lengths r_i and the asymmetric combinations S_a and S_b of the bond angles α_i ($i = 1, 2, 3$) defined as

$$S_a = \tfrac{1}{\sqrt{6}} \left[2\alpha_1 - \alpha_2 - \alpha_3\right], \tag{14}$$

$$S_b = \tfrac{1}{\sqrt{2}} \left[\alpha_2 - \alpha_3\right] \tag{15}$$

by expanding them in terms of the Cartesian displacements around the reference configuration and truncating after the first order, see Yurchenko et al. (2007).

The stretching basis functions $\phi_{v_1}(\xi_1^{\rm lin})$, $\phi_{v_2}(\xi_2^{\rm lin})$, and $\phi_{v_3}(\xi_3^{\rm lin})$, as well as the inversion basis functions $\phi_{v_6}(\xi)$ ($\xi = \delta$) are generated numerically using the Numerov–Cooley approach (Noumerov 1924; Cooley 1961), while for the bending basis functions $\phi_{v_4}(\xi_4^{\rm lin})$ and $\phi_{v_5}(\xi_5^{\rm lin})$, 1D Harmonic oscillator wavefunctions were used. These basis functions are then optimized via a contraction-symmetrization procedure (Yurchenko, Yachmenev & Ovsyannikov 2017) to form a symmetry adapted ($\mathcal{D}_{3h}$(M)) vibrational ($J = 0$) basis functions $\Phi_N^{\Gamma_{\rm vib}}$ as a sum-of-products of ϕ_{v_i} ($i = 1, \ldots, 6$). At this stage, the vibrational basis functions $\Phi_N^{\Gamma_{\rm vib}}$ are assigned the normal mode QNs n_1, n_2, $n_3^{l_3}$, and $n_4^{l_4}$ by correlating our local node wavefunctions ϕ_{v_i} to the Harmonic-oscillator-like solutions. For the rotational basis set, symmetrized rigid-rotor wavefunctions $|J, K, \Gamma_{\rm rot}\rangle$ as generated using simple Wang combinations, see equations (2) and (3). The rotational and vibrational assignments are then propagated to the final ro-vibrational variational wavefunctions using the largest eigencoefficient approach (Yurchenko 2023). The size of the vibrational basis set is controlled by the polyad number parameter P defined as

Table 8. Extract from the `.states` file of the $^{15}NH_3$ CoYuTe-15 line list.

i	$\tilde{E}$ (cm^{-1})	g	J	unc. (cm^{-1})	τ/s	$\Gamma_{\rm tot}$	n_1	n_2	n_3	l_3	n_4	l_4	$\Gamma_{\rm vib}$	K	$\Gamma_{\rm rot}$	N	s/a	$\lvert C_i^2\rvert$	v_1	v_2	v_3	v_4	v_5	v_6	Label	$\tilde{E}_{\rm calc.}$ (cm^{-1})
30257	16.904164	12	1	0.000141	6.8781E + 06	E'	0	0	0	0	0	0	A_2''	1	E'	1	a	1.00	0	0	0	0	0	1	IE	16.905288
30258	978.920185	12	1	0.000261	6.7761E − 02	E'	0	1	0	0	0	0	A_2''	1	E'	2	a	1.00	0	0	0	0	0	3	IE	978.913857
30259	1637.547381	12	1	0.000461	2.2083E − 01	E'	0	0	0	0	1	1	E'	1	E'	4	a	1.00	0	0	0	0	1	1	IE	1637.563266
30260	1643.458772	12	1	0.000424	2.1748E − 01	E'	0	0	0	0	1	1	E'	0	A_2'	4	s	1.00	0	0	0	0	1	0	IE	1643.466108
30261	1886.697223	12	1	0.000424	3.9163E − 02	E'	0	2	0	0	0	0	A_2''	1	E'	3	a	1.00	0	0	0	0	0	5	IE	1886.683504
30262	2553.937518	12	1	0.000616	5.2107E − 02	E'	0	1	0	0	1	1	E'	0	A_2'	6	s	1.00	0	0	0	0	1	2	IE	2553.902032
30263	2590.898376	12	1	0.000848	5.1537E − 02	E'	0	1	0	0	1	1	E'	1	E'	6	a	1.00	0	0	0	0	1	3	IE	2590.901311
30264	2891.605307	12	1	0.000616	2.3392E − 02	E'	0	3	0	0	0	0	A_2''	1	E'	5	a	1.00	0	0	0	0	0	7	IE	2891.589118
30265	3199.900421	12	1	0.401000	4.0453E − 02	E'	0	2	0	0	1	1	E'	0	A_2'	7	s	0.99	0	0	0	0	1	4	Ca	3199.900421
30266	3228.710631	12	1	0.201000	1.0889E − 01	E'	0	0	0	0	2	0	A_2''	1	E'	8	a	0.99	0	0	0	0	2	1	Ca	3228.710631
30267	3254.708183	12	1	0.401000	1.0861E − 01	E'	0	0	0	0	2	2	E'	0	A_2'	9	s	1.00	0	0	0	0	2	0	Ca	3254.708183
30268	3257.325527	12	1	0.401000	1.0759E − 01	E'	0	0	0	0	2	2	E'	1	E'	9	a	0.99	0	0	0	0	2	1	Ca	3257.325527
30269	3350.280661	12	1	0.002106	1.0758E − 01	E'	1	0	0	0	0	0	A_2''	1	E'	10	a	1.00	1	0	0	0	0	1	IE	3350.267395

Notes. i: state identifier; $\tilde{E}$: state term value; g: state degeneracy; J: state rotational QN; unc.: energy uncertainty; τ: lifetime; $\Gamma_{\rm tot}$: total symmetry in $\mathcal{D}_{3h}$ (M); n_1, n_2, n_3, l_3n_4, l_4: normal mode vibrational QNs; $\Gamma_{\rm vib}$: symmetry of vibrational contribution in $\mathcal{D}_{3h}$(M); K: rotational QN; $\Gamma_{\rm rot}$: symmetry of rotational contribution in $\mathcal{D}_{3h}$ (M); N: vibrational state ID; $|C_i^2|$: largest coefficient used in the assignment; $v_1 - v_6$: TROVE vibrational QN; Label: label indicating if the term value is based on the MARVEL ('Ma') isotope extrapolation ('IE') or the CoYuTe-15 energy list ('Ca'); $\tilde{E}_{\rm calc.}$: original CoYuTe-15 state term value.

Table 9. Extract from a `.trans` file of the $^{15}NH_3$ CoYuTe-15 line list.

f	i	A_{fi}
1834174	2006561	4.8904E − 05
6245112	6543052	6.5693E − 05
2454658	3091139	3.7242E − 12
345773	154525	8.1452E + 00
3554160	3317840	9.4551E − 19
939596	816387	7.1870E − 02
8989567	9887870	1.0556E − 17
509601	419435	4.0892E − 12

Notes. f: upper state counting number; i: lower state counting number; A_{fi}: Einstein- Acoefficient (in s^{-1}).

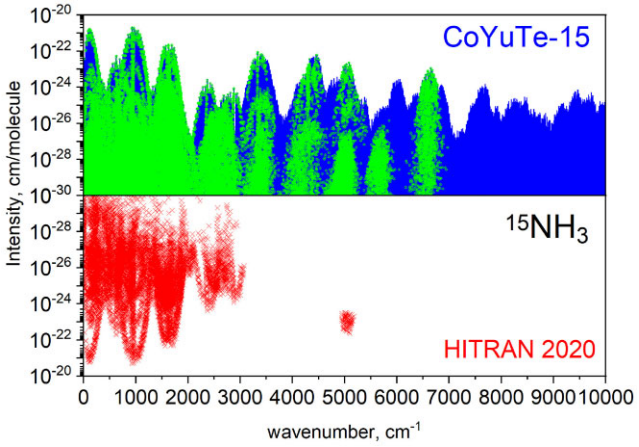

Figure 5. Comparison of the CoYuTe-15 spectrum (scaled to natural abundance) with HITRAN 2000 (Gordon et al. 2022) at $T = 296$ K. Green (lighter) points indicate 53 856 transitions connecting MARVEL states only.

follows:

$$P = 2(v_1 + v_2 + v_3) + v_4 + v_5 + v_6 = 2(n_1 + n_3) + n_2 + n_4 \leq P_{\rm max}. \tag{16}$$

As in Coles et al. (2019), $P_{\rm max} = 17$ was used. Another parameter controlling the ro-vibrational basis set size is the energy threshold $E_{\rm max} = 30000$ cm^{-1}. For the zero-point energy defined at the energy of the (non-physical) $J = 0$, $K = 0$, s, and $N = 1$ state relative to the minimum of the CoYuTe PES NH_3 (Coles et al. 2019), we obtained 8001.42 cm^{-1}.

Fig. 3 shows how the calculated energy values with TROVE compare to the experimentally derived energy term values of $^{15}NH_3$ (MARVEL) as obs. − calc. residuals. The majority of the residuals are below 0.1 cm^{-1}. The majority of the values with large residuals correspond to the MARVEL energies based on 1–2 transitions only.

5.2 Pseudo-MARVEL: isotopologue energy extrapolation

One of the limitations of the MARVEL technique is that the completeness of the MARVEL energies depends on the completeness of the original experimental sources. It is not uncommon for the experimental data set to be patchy, with some lines missing, with ambiguous assignment or blended transitions. In attempt to fill gaps in the MARVEL energy sets when MARVELizing the line lists, different techniques can be employed (McKemmish et al. 2024). Here, we consider the isotopologue energy level extrapolation technique, similar to the one employed in Polyansky et al. (2017), where we leverage the present MARVEL energy levels list for the $^{14}NH_3$ parent isotopologue (Furtenbacher et al. 2020). The IE technique uses the assumption that the calculation errors of ro-vibrational energies of different isotopologues based on the same Born–Oppenheimer PES are approximately uniform.

To this end, variational TROVE calculations are performed using the *ab initio* surface from Polyansky et al. (2016), for both the $^{14}NH_3$ and $^{15}NH_3$ isotopologues. The *ab initio* ro-vibrational energies from both isotopologues are then matched to their corresponding MARVEL energies from this study and on the parent isotopologue from Furtenbacher et al. (2020). Here, we opt for the *ab initio* PESs in place of (more accurate) empirical PESs in order to mitigate possible contamination of the Born–Oppenheimer original *ab initio* surface with any mass dependent effects absorbed into CoYuTe PES through fitting to the experiment in Coles et al. (2019). The *ab initio* residuals $\Delta\tilde{E} = \tilde{E}^{\rm obs.} - \tilde{E}^{\rm calc.}$ (observed minus calculated) of each energy level included in MARVEL are first computed for the main isotopologue $^{14}NH_3$ and then these obs. − calc. differences are added onto the *ab initio* energies of $^{15}NH_3$. In this way, we form IE (McKemmish et al. 2024) MARVEL levels for $^{15}NH_3$ enabling a semi-empirical determination of energy levels present in the $^{14}NH_3$MARVEL list but not yet determined for $^{15}NH_3$.

To gauge the accuracy of the IE levels for $^{15}NH_3$, we compare those levels present in our MARVEL study, with their IE counterparts. The residuals between the MARVEL energies $^{15}NH_3$ and the CoYuTe-15 computed energies alongside the residuals of IE energies are given in Fig. 4. As can be seen, the difference in accuracy between the two is found to vary, and shows a vibrational dependence. For this reason,

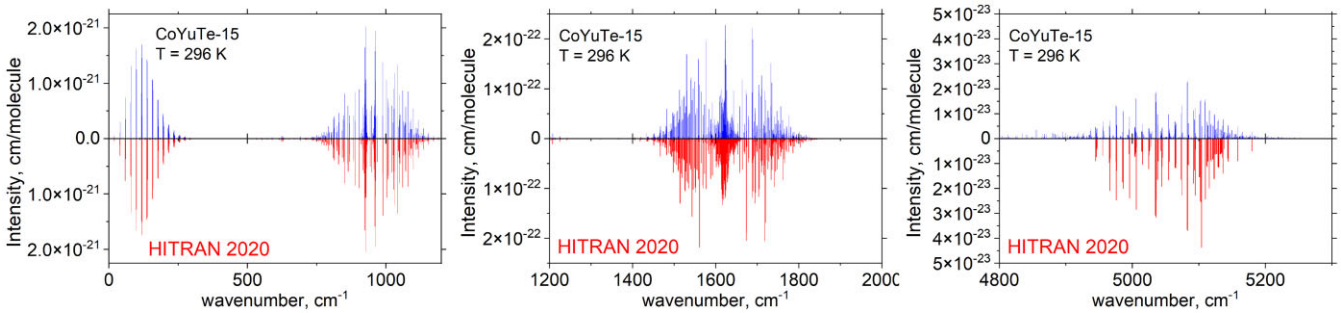

Figure 6. Comparison of the CoYuTe-15 spectrum with HITRAN 2000 (Gordon et al. 2022) at $T = 296$ K.

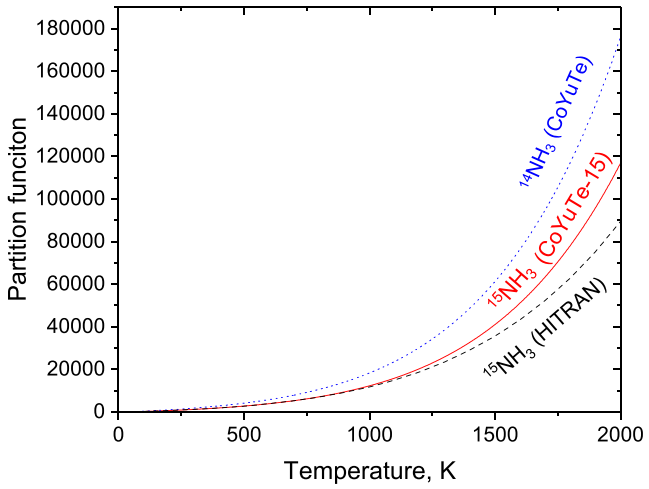

Figure 7. The partition function of $^{15}NH_3$ (CoYuTe-15) from this work (solid line) is compared to the HITRAN (TIPS) partition function of $^{15}NH_3$ (Gamache et al. 2017, dashed line) as well to the partition function of $^{14}NH_3$ from the CoYuTe line lists (dotted line).

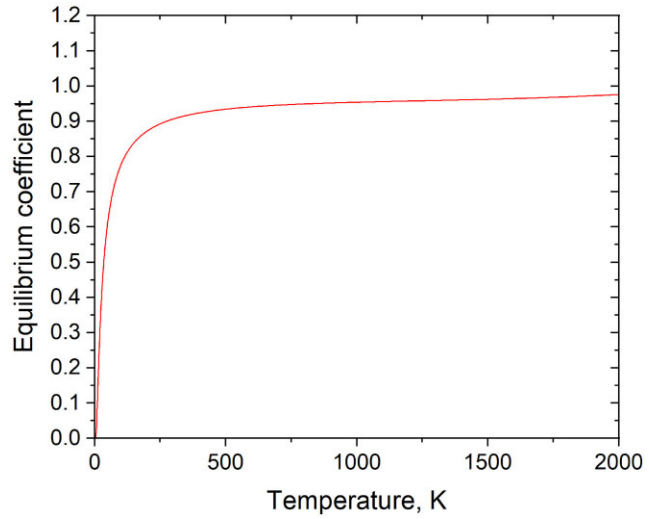

Figure 8. Equilibrium constants of the reaction in equation (17) as function of T.

we only substitute IE levels in place of CoYuTe-15 levels for bands which are known to provide increased accuracy over CoYuTe-15. For excited vibrational states, the only IE levels found to improve over CoYuTe-15 belong to the g.s., the ν_2 inversion mode and its overtones, $2\nu_2$ and $3\nu_2$, summarized in Table 6, and indicated in Fig. 4 as 'IE Chosen'. The corresponding uncertainties, also listed in Table 7, were estimated by comparing to the MARVEL values if available, which are indicated in Fig. 4 as 'IE Excluded'.

5.3 Line list

The CoYuTe-15 line list for $^{15}NH_3$ was computed for $J = 0, \ldots, 30$ covering the wavenumber range up to 10 000 cm^{-1}, with the upper/lower energies limited by 18 000/8000 cm^{-1}, respectively. Intensity (Einstein A coefficients) calculations were performed on a GPU cluster using the GAIN MPI code (Al-Refaie, Yurchenko & Tennyson 2017).

The line list contains 929 795 249 transitions between 12 699 617 ro-vibrational states and consists of a States file, Transitions files, and Partition function file. According with the ExoMolHD standards (Tennyson et al. 2020), we use experimentally derived energies to replace the theoretical values, where available, the procedure commonly referenced to as 'MARVELization'. From the MARVEL set of 2777 energies, we selected 2754 values with residuals smaller than 1 cm^{-1} from the TROVE energy term value to avoid any accidental MARVEL outliers. These were complemented by 326 IE values and finally with a 14 $J = 18$ effective Hamiltonian term values from Urban et al. (1985a).

Extracts from the States and Transition files are illustrated in Tables 8 and 9. We follow the energy convention used for ammonia, where the lowest energy is the energy of the non-physical g.s. $J = 0$, $K = 0$, s, and A_1' (0,0,0^0, 0^0), which is set to zero. In this convention, the lowest observable state $J = 0$, $K = 0$, a, and A_2'' (0,0,0^0, 0^0) has the energy of the inversion splitting, which we set to 0.757685 cm^{-1} (Urban et al. 1985a). Therefore the MARVEL energies, which are based on a different contention for the lowest ro-vibrational energy, are shifted by 0.757685 cm^{-1} before using them in the MARVELization procedure. For practical purposes, we keep the non-existing $J = 0$ energies in the .states file, which are however 'switched-off' from any intensity applications by setting the corresponding degeneracy factors g to zero.

In Fig. 5, an overview of the new line list is presented in a form of a room temperature (296 K) stick spectrum compared to the HITRAN 2020 $^{15}NH_3$ data (Gordon et al. 2022). Using the MARVELized energies only, we obtain 53 856 CoYuTe-15 transitions with intensities above 10^{-30} cm^2 molecule^{-1} after scaling to terrestrial (natural) abundance as taken from . This is to compare to 13 792 $^{15}NH_3$ transitions in HITRAN 2020, mostly covering the wavenumber region below 3500 cm^{-1}. Fig. 6 offers a more detailed comparison of the CoYuTe-15 $T = 296$ K spectrum with HITRAN 2020 in the three spectroscopic windows showing four bands, assuming

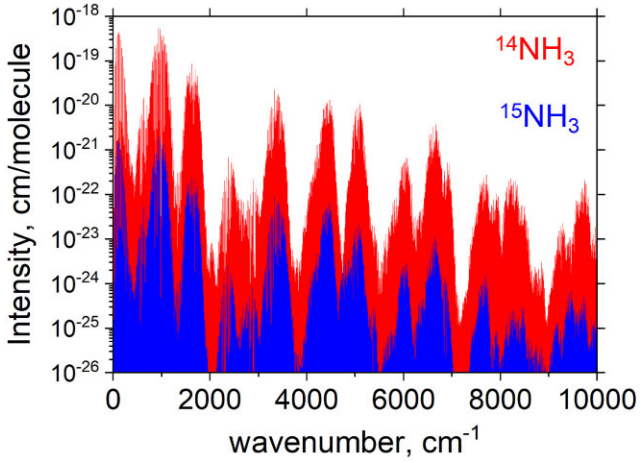

Figure 9. Room temperature intensities of $^{15}NH_3$ relative to that of $^{14}NH_3$, scaled to the corresponding natural abundances, 3.66129×10^{-3} and 0.995872, respectively. The $^{14}NH_3$ intensities are computed using the CoYuTe line list (Coles et al. 2019).

natural abundances. This high-resolution $^{15}NH_3$MARVEL line list in the HITRAN format is provided as Supporting Information.

Partition functions of $^{15}NH_3$ (CoYuTe-15) and $^{14}NH_3$ (CoYuTe) are compared in Fig. 7, where we also show the HITRAN partition function of $^{15}NH_3$ from TIPS (Total Internal Partition Sums, Gamache et al. 2021). The latter is significantly smaller due to insufficient number of vibrational states used.

Using these these two CoYuTe partition functions of $^{15}NH_3$ and $^{14}NH_3$, we evaluated their equilibrium constants corresponding to the atomization reaction

$$^{15}\mathrm{N} + {}^{14}\mathrm{NH_3} \longrightarrow {}^{14}\mathrm{N} + {}^{15}\mathrm{NH_3}. \quad (17)$$

For the reaction

$$\mathrm{A} + \mathrm{B} \longrightarrow \mathrm{C} + \mathrm{D} \quad (18)$$

we evaluate the temperature dependent equilibrium constant as follows (Hewitt et al. 2005)

$$K = \left(\frac{m_\mathrm{A} m_\mathrm{B}}{m_\mathrm{C} m_\mathrm{D}}\right)^{3/2} \frac{Q_\mathrm{A} Q_\mathrm{B}}{Q_\mathrm{C} Q_\mathrm{D}} \exp\left(-\frac{c_2 \tilde{U}}{T}\right), \quad (19)$$

where Q_A and Q_C are atomic partition functions assumed to be 2 and 3 for ^{15}N and ^{14}N, respectively, Q_B and Q_D are the internal partition functions of $^{14}NH_3$ and $^{15}NH_3$, respectively, and c_2 is the second radiative constant (K/cm^{-1}). The enthalpy of the reaction $\tilde{U}$ (cm^{-1}) is given by

$$\tilde{U} = E_0^\mathrm{D} - E_0^\mathrm{B},$$

where E_0^B ($^{14}NH_3$) and E_0^D($^{15}NH_3$) are the molecular zero-point energies, 8017.6 and 8001.42 cm^{-1}, respectively. The temperature dependence of K for this reaction is illustrated in Fig. 8. It is close to 1 at moderate and high temperatures but exhibits drastic variation at very low values of T.

Fig. 9 shows how the intensities of $^{15}NH_3$ compare to $^{14}NH_3$ assuming natural abundances. The majority of the region is well above 10^{-26} cm molecule^{-1}. In Fig. 10, the cumulative density of energy sources for each transition is plot as a function of transition intensity for the CoYuTe-15 line list at 296 K. This figure demonstrates that essentially all transitions with intensity above 10^{-20} cm molecule^{-1} have both lower and upper energy levels accounted for in the MARVEL analysis. Even at 10^{-22} cm molecule^{-1}, approximately half of the transitions are accounted for in the MARVEL analysis.

Cacciani et al. (2022) reported spectra of ammonia in the 3900 and 4700 cm^{-1} region with a detailed analysis and assignment of $^{14}NH_3$ lines. The spectra contains also lines of $^{15}NH_3$, which have not been assigned yet. In Fig. 11, we compare our theoretical lines of $^{15}NH_3$ at $T = 296$ K to the experimental spectral lines from Cacciani et al. (2022). Here, the intensities were scaled to the abundance of 5.7×10^{-3} suggested by Cacciani et al. (2022). For a detailed analysis, six strong lines from the latter work were selected, analysed and compared to the CoYuTe-15 values in Table 10. The agreement of the line positions is well within 0.001 cm^{-1} for the MARVELized values and within 0.02 cm^{-1} for the calculated ones. The intensity ratios vary from ≈75 per cent (weaker band $\nu_1 + \nu_2$) to up to ≈

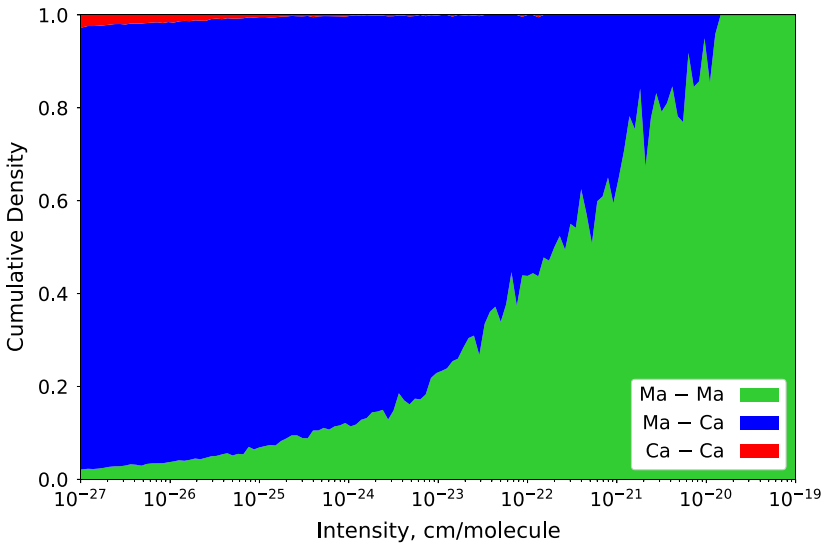

Figure 10. The cumulative density of energy sources for each transition as a function of transition intensity at 296 K. The Ma–Ca and Ca–Ma transitions are grouped together in one region Ma-Ca. The abbreviations Ma and Ca denote emperical (MARVEL) and variational (calculated) methodologies, respectively. The $^{15}NH_3$ abundance of 1 was assumed.

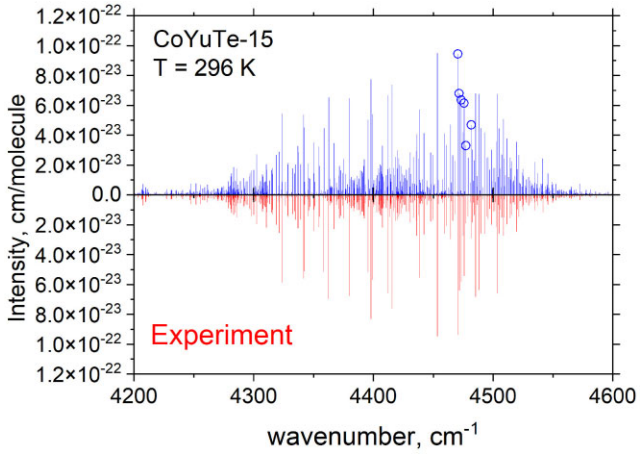

Figure 11. Comparison of the CoYuTe-15 spectrum in the 4400 cm^{-1} window with the unassigned experimental spectrum by Cacciani et al. (2022) at $T = 296$ K. The theoretical spectrum is scaled to the abundance by 5.7×10^{-3} suggested by Cacciani et al. (2022). Circles indicate lines selected for a detailed comparison in Table 10.

15 per cent (stronger band $\nu_2 + \nu_3$). This agreement between theory and experiment shows that CoYuTe-15 can be very useful as a starting point for formally assigning this spectrum.

5.4 Collisional line-broadening

Line-broadening parameters are an essential part of a spectroscopic data base required to produce molecular cross-sections. As part of the new line list for $^{15}NH_3$, here we update the ammonia line line-broadening parameters applicable both to $^{14}NH_3$ and $^{15}NH_3$. This is in line with the ExoMol line broadening 'diet' adopted in Barton et al. (2017). Collisional line-broadening of $^{14}NH_3$ has been extensively studied in the past, with a special attention to the microwave inversion spectra that exhibits its own peculiarities (Ben-Reuven 1966; Skinner, Hargreaves & Gordon 2022). A review of available broadening data in the infrared by molecular hydrogen and helium was made by HITRAN (Wilzewski et al. 2016). Little vibrational dependence is observed for these perturbers, so only rotational dependence of broadening parameters is considered here. For H_2 broadening coefficients γ, a polynomial in m and K, first appearing in Nemtchinov, Sung & Varanasi (2004), is adopted to describe the rotational dependence in terms of QN K and rotational line index m. We introduce one change to this polynomial, namely using the absolute value of $|m|$ instead of m to ensure correct behaviour in P- and R-branches. The spectroscopic coefficient m is defined as $-J''$ for P-branch and $J''+1$ for R-branch.

The single-power law is assumed for the temperature dependence of $\gamma(T)$:

$$\gamma(T) = \gamma_0(T_{\rm ref})\left(\frac{T_{\rm ref}}{T}\right)^n, \tag{20}$$

where n is the temperature exponent and $\gamma_0(T_{\rm ref})$ is the half-width at-half-maximum of the line at the reference temperature.

Here, we provide two ExoMol broadening 'diets' for NH_3 in the form of `.broad` files. The first one uses the `m0` diet (Tennyson et al. 2024b) represented by the m-dependence only with dependencies on all other QNs averaged. We also give a version with the `m1` diet, with $\gamma = \gamma(|m|, K'')$, that is, m and K'' dependent, which should provide a more accurate description of NH_3 line shapes broadened by H_2. Although broadening coefficients for various K can substantially differ (see Fig. 12), the non-rigorous quantum rotational number K is not always well characterized and therefore the `m0` diet can be more practical. Wherever this assignment is known and reliable, the `m1` diet can be used as a more complete representation of the broadening parameters.

Helium-broadening parameters show little variation even against the rotational variable m, so the `m0` diet should suffice. The `m1` diet for this broadener is still provided for the sake of completeness. To construct the `m`-diets helium-broadening, the HITRAN data (Wilzewski et al. 2016) for γ and n were used. These data are based on $^{14}NH_3$ measurements, but should also work well for broadening of $^{15}NH_3$. Nemtchinov et al. (2004) estimate that the broadening parameters for both isotopologues are within 3 per cent at the measured temperatures; this is well below the uncertainties associated with the current parametrizations of γ and n.

6 CONCLUSIONS

An extensive ExoMol line list CoYuTe-15 for the isotopologue of $^{15}NH_3$ CoYuTe-15 is presented. The line list was computed with the variational program TROVE using the spectroscopic model (empirical PES and *ab initio* DMS) of NH_3 developed and used for production of a hot line list of $^{14}NH_3$ by Coles et al. (2019). The line list covers the wavenumber range up to 10 000 cm^{-1} and the rotational excitations up to $J = 30$. In order to improve the variational energies, a set of 2777 empirically derived energy levels of $^{15}NH_3$ was constructed using the MARVEL procedure and used to replace the theoretical energies where possible. On top of that, we used an IE technique (Polyansky et al. 2017) to generate energies for states not covered by the $^{15}NH_3$MARVEL, but featured in the $^{14}NH_3$MARVEL set (Furtenbacher et al. 2020). This IE technique was applied to fill the gaps in the MARVEL energies from the g.s., ν_2,

Table 10. Comparison of line positions and intensities ($T = 296$ K) for six selected lines from the experimental spectrum by Cacciani et al. (2022), see lines indicated with circles in Fig. 11. The theoretical spectrum is scaled to the abundance by 5.7×10^{-3} suggested by Cacciani et al. (2022). The labels 'Ma' and 'Ca' indicate if the line position values are from MARVEL or calculated.

		Positions (cm^{-1})				Intensities (10^{-23} cm molecule^{-1})		
Line	Band	Obs.	Calc.	Obs. − calc.	Ma/Ca	Obs.	Calc.	Ratio (calc./obs.)
$^{R}R(3,3)$	$\nu_2+\nu_3$	4470.52292	4470.52222	0.00070	Ma	9.36	9.44	1.01
$^{R}R(4,3)$	$\nu_2+\nu_3$	4471.65737	4471.67685	−0.01948	Ca	6.39	6.80	1.06
$^{R}R(2,0)$	$\nu_2+\nu_3$	4473.32228	4473.32191	0.00037	Ma	5.82	6.37	1.10
$^{R}R(3,0)$	$\nu_2+\nu_3$	4475.73941	4475.73901	0.00040	Ma	5.43	6.16	1.13
$^{R}R(3,2)$	$\nu_1+\nu_2$	4477.11327	4477.11322	0.00005	Ma	1.89	3.31	1.75
$^{R}R(4,4)$	$\nu_1+\nu_2$	4481.68651	4481.69588	−0.00937	Ca	2.91	4.69	1.61

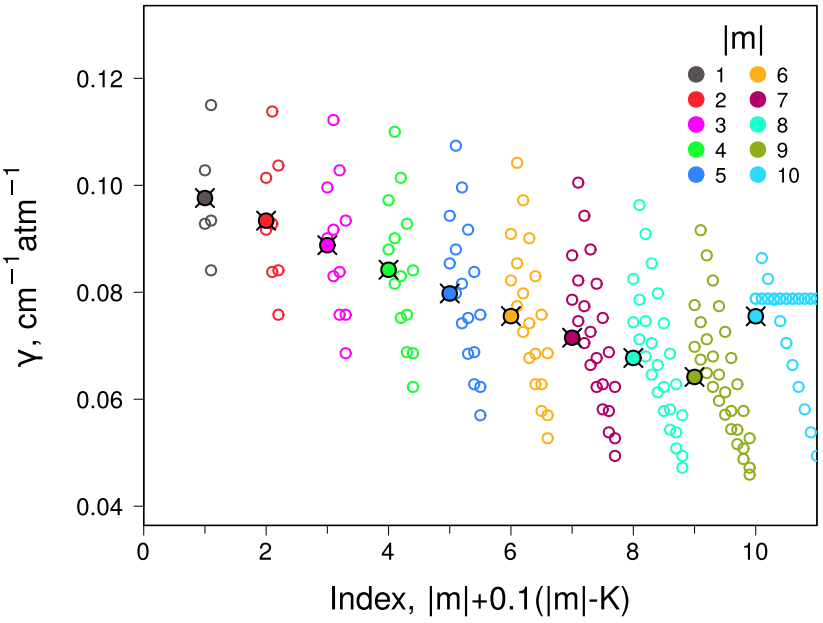

Figure 12. Collisional broadening parameters for the NH_3–H_2 system. Empty circles are HITRAN data for lines with various rotational assignments $\{m, K''\}$, and filled-in circles are their K-averages (`m1` diet).

$2\nu_2$, and $3\nu_2$. We show that the line list is sufficiently accurate to help assign the existing experimental spectra of $^{15}NH_3$ as well to facilitate future spectroscopic analyses and astronomical detections. The line list as well as the spectroscopic model can be obtained at www.exomol.com.

ACKNOWLEDGEMENTS

We thank Sammy Akkouche and Isabella Freitas for help at the start of the project. This work was supported by the STFC projects nos ST/R000476/1 and ST/Y001508/1. The authors acknowledge the use of the UCL Legion High Performance Computing Facility (Legion@UCL) and associated support services in the completion of this work, along with the Cambridge Service for Data Driven Discovery (CSD3) and the DiRAC Data Intensive service DIaL2.5 at the University of Leicester, managed on behalf of the STFC DiRAC HPC Facility (www.dirac.ac.uk). These DiRAC services were funded by BEIS, UKRI, and STFC capital funding and STFC operations grants. DiRAC is part of the UKRI Digital Research Infrastructure. This work was also supported by the European Research Council (ERC) under the European Union's Horizon 2020 research and innovation programme through Advance grant no. 883830.

DATA AVAILABILITY

The data underlying this article are available in the article and in its online Supporting Information. The line list and associated data are available from www.exomol.com. The codes used in this work, namely TROVE and EXOCROSS, are freely available via https://github.com/exomol.

REFERENCES

Al Derzi A. R., Furtenbacher T., Yurchenko S. N., Tennyson J., Császár A. G., 2015, J. Quant. Spectrosc. Radiat. Transfer, 161, 117
Al-Refaie A. F., Yurchenko S. N., Tennyson J., 2017, Comput. Phys. Commun., 214, 216
Anders S., Jonuscheit J., Lehner U., Sarka K., Schrotter H. W., 2000, J. Raman Spectrosc., 31, 711
Barrado D. et al., 2023, Nature, 624, 263
Barton E. J., Hill C., Czurylo M., Li H.-Y., Hyslop A., Yurchenko S. N., Tennyson J., 2017, J. Quant. Spectrosc. Radiat. Transfer, 203, 490
Ben-Reuven A., 1966, Phys. Rev., 145, 7
Brown L., Margolis J., 1996, J. Quant. Spectrosc. Radiat. Transfer, 56, 283
Buffa G., Lucchesi M., Tarrini O., Martinelli M., 1994, J. Quant. Spectrosc. Radiat. Transfer, 52, 673
Bunker P. R., Jensen P., 1998, Molecular Symmetry and Spectroscopy, 2nd edn. NRC Research Press, Ottawa
Cacciani P., Cermak P., Vander Auwera J., Campargue A., 2022, J. Quant. Spectrosc. Radiat. Transfer, 277, 107961
Canè E., Di Lonardo G., Fusina L., Tamassia F., Predoi-Cross A., 2019, J. Chem. Phys., 150, 194301
Canè E., Lonardo G. D., Fusina L., Tamassia F., Predoi-Cross A., 2020, J. Quant. Spectrosc. Radiat. Transfer, 250, 106987
Carlotti M., Trombetti A., Velino B., Vrbancich J., 1980, J. Mol. Spectrosc., 83, 401
Čermák P., Hovorka J., Veis P., Cacciani P., Cosléou J., Romh J. E., Khelkhal M., 2014, J. Quant. Spectrosc. Radiat. Transfer, 137, 13
Charnley S. B., Rodgers S. D., 2002, ApJ, 569, L133
Chu F. Y., Freund S. M., 1973, J. Mol. Spectrosc., 48, 183
Cohen E. A., 1980, J. Mol. Spectrosc., 79, 496
Coles P. A., Ovsyannikov R. I., Polyansky O. L., Yurchenko S. N., Tennyson J., 2018, J. Quant. Spectrosc. Radiat. Transfer, 219, 199
Coles P. A., Yurchenko S. N., Tennyson J., 2019, MNRAS, 490, 4638
Cooley J. W., 1961, Math. Comp., 15, 363
Császár A. G., Furtenbacher T., 2011, J. Mol. Spectrosc., 266, 99
Császár A. G., Czakó G., Furtenbacher T., Mátyus E., 2007, Annu. Rep. Comput. Chem., 3, 155
D'Cunha R., 1987, J. Mol. Spectrosc., 122, 130
D'Cunha R., Urban S., Rao K. N., Henry L., Valentin A., 1985, J. Mol. Spectrosc., 111, 352
Devi V. M., Rao K. N., Pracna P., Urban S., 1990, J. Mol. Spectrosc., 143, 18
Di Lonardo G., Fusina L., Trombetti A., Mills I. M., 1982, J. Mol. Spectrosc., 92, 298

Down M. J., Hill C., Yurchenko S. N., Tennyson J., Brown L. R., Kleiner I., 2013, J. Quant. Spectrosc. Radiat. Transfer, 130, 260
Fletcher L. N., Greathouse T., Orton G., Irwin P., Mousis O., Sinclair J., Giles R., 2014, Icarus, 238, 170
Földes T., Vanfleteren T., Rizopoulos A., Herman M., Vander Auwera J., Softley T., Di Lonardo G., Fusina L., 2016, J. Quant. Spectrosc. Radiat. Transfer, 179, 112
Fouchet T., Lellouch E., Bezard B., Encrenaz T., Drossart P., Feuchtgruber H., de Graauw T., 2000, Icarus, 143, 223
Fouchet T., Irwin P. G. J., Parrish P., Calcutt S. B., Taylor F. W., Nixon C. A., Owen T., 2004, Icarus, 172, 50
Freund S. M., Oka T., 1976, Phys. Rev. A, 13, 2178
Furtenbacher T., Császár A. G., 2012a, J. Quant. Spectrosc. Radiat. Transfer, 113, 929
Furtenbacher T., Császár A. G., 2012b, J. Mol. Struct., 1009, 123
Furtenbacher T., Császár A. G., Tennyson J., 2007, J. Mol. Spectrosc., 245, 115
Furtenbacher T., Árendás P., Mellau G., Császár A. G., 2014, Sci. Rep., 4, 4654
Furtenbacher T., Coles P. A., Tennyson J., Yurchenko S. N., Yu S., Drouin B., Tóbiás R., Császár A. G., 2020, J. Quant. Spectrosc. Radiat. Transfer, 251, 107027
Gamache R. R. et al., 2021, J. Quant. Spectrosc. Radiat. Transfer, 271, 107713
Gamache R. R. et al., 2017, J. Quant. Spectrosc. Radiat. Transfer, 203, 70
Gerin M., Marcelino N., Biver N., Roueff E., Coudert L. H., Elkeurti M., Lis D. C., Bockelee-Morvan D., 2009, A&A, 498, L9
Good W. E., Coles D. K., 1947, Phys. Rev., 71, 383
Gordon I. E. et al., 2022, J. Quant. Spectrosc. Radiat. Transfer, 277, 107949
Harper L. A., Sharpe R. R., 1998, Atmos. Environ., 32, 273
Hewitt A. J., Doss N., Zobov N. F., Polyansky O. L., Tennyson J., 2005, MNRAS, 356, 1123
Huang X., Schwenke D. W., Lee T. J., 2011a, J. Chem. Phys., 134, 044320
Huang X., Schwenke D. W., Lee T. J., 2011b, J. Chem. Phys., 134, 044321
Huttner W., Frank U., Nowicki P., 1992, Chem. Phys. Lett., 196, 614
Jones H., 1978, J. Mol. Spectrosc., 70, 279
Karyakin E. N., Krupnov A. F., Papoušek D., Shchurin J. M., Urban S., 1977, J. Mol. Spectrosc., 66, 171
Kefala K., Boudon V., Yurchenko S. N., Tennyson J., 2024, J. Quant. Spectrosc. Radiat. Transfer, 316, 108897
Lees R. M., Li L., Liu Z., Xu L.-H., 2006, J. Mol. Struct., 795, 134
Lees R. M., Li L., Xu L.-H., 2008, J. Mol. Spectrosc., 251, 241
Li L., Lees R. M., Xu L.-H., 2007, J. Mol. Spectrosc., 243, 219
Lis D. C., Wootten A., Gerin M., Roueff E., 2010, ApJ, 710, L49
McKemmish L. K., Bowesman C. A., Kefala K., Perri A. N., Syme A. M., Yurchenko S. N., Tennyson J., 2024, RAS Tech. Instrum., in press
Moriwaki Y., Nakagawa K., Shimizu T., 1991, Japan. J. Appl. Phys. 1, 30, 2901
Mumma M. J., Charnley S. B., 2011, ARA&A., 49, 471
Nemtchinov V., Sung K., Varanasi P., 2004, J. Quant. Spectrosc. Radiat. Transfer, 83, 243
Noumerov B. V., 1924, MNRAS, 84, 592
Pizzarello S., Williams L. B., 2012, ApJ, 749, 161
Polyansky O. L., Ovsyannikov R. I., Kyuberis A. A., Lodi L., Tennyson J., Yachmenev A., Yurchenko S. N., Zobov N. F., 2016, J. Mol. Spectrosc., 327, 21
Polyansky O. L., Kyuberis A. A., Lodi L., Tennyson J., Yurchenko S. N., Ovsyannikov R. I., Zobov N. F., 2017, MNRAS, 466, 1363
Redaelli E., Bizzocchi L., Caselli P., Pineda J., 2023, A&A, 674, L8
Sasada H., 1980, J. Mol. Spectrosc., 83, 15
Sasada H., Schwendeman R. H., 1986, J. Mol. Spectrosc., 117, 331
Sasada H., Hasegawa Y., Amano T., Shimizu T., 1982, J. Mol. Spectrosc., 96, 106
Sattler J., Worchesky T., 1981, J. Mol. Spectrosc., 90, 297
Schatz W., Renk K. F., Fusina L., Izatt J. R., 1994, Appl. Phys. B, 59, 453
Schilke P., Walmsley C. M., Mauersberger R., 1991, A&A, 247, 516
Shojachaghervand P., Schwendeman R. H., 1983, J. Mol. Spectrosc., 97, 306
Skinner F. M., Hargreaves R. J., Gordon I. E., 2022, MNRAS, 514, 2864
Tennyson J. et al., 2020, J. Quant. Spectrosc. Radiat. Transfer, 255, 107228
Tennyson J., Furtenbacher T., Yurchenko S. N., Császár A. G., 2024a, J. Quant. Spectrosc. Radiat. Transfer, 316, 108902
Tennyson J. et al., 2024b, J. Quant. Spectrosc. Radiat. Transfer, 326, 109083
Tóbiás R., Furtenbacher T., Tennyson J., Császár A. G., 2019, Phys. Chem. Chem. Phys., 21, 3473
Urban S., Papoušek D., Belov S. P., Krupnov A. F., Tretyakov M. Y., Yamada K., Winnewisser G., 1983, J. Mol. Spectrosc., 101, 16
Urban S., D'Cunha R., Rao K. N., 1984, J. Mol. Spectrosc., 106, 64
Urban S., D'Cunha R., Rao K. N., Papoušek D., 1985a, J. Mol. Spectrosc., 111, 361
Urban S., Misra P., Rao K. N., 1985b, J. Mol. Spectrosc., 114, 377
Urban S., D'Cunha R., Manheim J., Rao K. N., 1986, J. Mol. Spectrosc., 118, 298
Urban S., Klee S., Yamada K. M. T., 1994, J. Mol. Spectrosc., 168, 384
Wilzewski J. S., Gordon I. E., Kochanov R. V., Hill C., Rothman L. S., 2016, J. Quant. Spectrosc. Radiat. Transfer, 168, 193
Yurchenko S. N., 2015, J. Quant. Spectrosc. Radiat. Transfer, 152, 28
Yurchenko S., 2023, Computational Spectroscopy of Polyatomic Molecules. CRC Press, Boca Raton
Yurchenko S. N., Carvajalz M., Jensen P., Lin H., Zheng J. J., Thiel W., 2005, Mol. Phys., 103, 359
Yurchenko S. N., Thiel W., Jensen P., 2007, J. Mol. Spectrosc., 245, 126
Yurchenko S. N., Barber R. J., Yachmenev A., Thiel W., Jensen P., Tennyson J., 2009, J. Phys. Chem. A, 113, 11845
Yurchenko S. N., Yachmenev A., Ovsyannikov R. I., 2017, J. Chem. Theory Comput., 13, 4368

SUPPORTING INFORMATION

Supplementary data are available at *MNRAS* online.

The following is provided as supporting information (1) the MARVEL input (transitions and segment) file, output (energy) file, and an auxiliary 'segment' file containing the units description of the transition frequencies from the original sources and (2) a list of HITRAN-formatted high-resolution transitions of $^{15}NH_3$ computed at $T = 296$ K using the CoYuTe-15 intensities and the MARVEL energies.

Please note: Oxford University Press is not responsible for the content or functionality of any supporting materials supplied by the authors. Any queries (other than missing material) should be directed to the corresponding author for the article.

This paper has been typeset from a TEX/LATEX file prepared by the author.